Welcoming gallium- and indium-fumarate MOFs to the family

Zhang, Yue; Lucier, Bryan E. G.; Mckenzie, Sarah M.; Arhangelskis, Mihails; Morris, Andrew J.; Friščić, Tomislav; Reid, Joel W.; Terskikh, Victor V.; Chen, Mansheng; Huang, Yining

DOI:
10.1021/acsami.8b08562

Welcoming Gallium- and Indium-fumarate MOFs to the Family: Synthesis, Comprehensive Characterization, Observation of Porous Hydrophobicity, and CO_2 Dynamics

Yue Zhang,[a] Bryan E. G. Lucier,[a] Sarah M. McKenzie,[a] Mihails Arhangelskis,[b] Andrew J. Morris,[c] Tomislav Friščić,[b] Joel Reid,[d] Victor V. Terskikh,[e] Mansheng Chen,[a] Yining Huang[a,]*

[a] *Department of Chemistry, The University of Western Ontario, London, Ontario, Canada N6A 5B7*

[b] *Department of Chemistry, McGill University, 801 Sherbrooke Street West, Montréal, Québec, Canada H3A 0B8*

[c] *School of Metallurgy and Materials, University of Birmingham, Edgbaston, Birmingham B15 2TT, UK*

[d] *Canadian Light Source, 44 Innovation Boulevard, Saskatoon, Saskatchewan, Canada S7N 2V3*

[e] *Department of Chemistry, University of Ottawa, 10 Marie Curie Private, Ottawa, Ontario, Canada K1N 6N5*

**Corresponding author, E-mail: yhuang@uwo.ca, webpage: http://publish.uwo.ca/~yhuang/*

Abstract

The properties and applications of metal-organic frameworks (MOFs) are strongly dependent on the nature of the metals and linkers employed, along with the specific conditions employed during synthesis. Al-fumarate, trademarked as Basolite A520, is a porous MOF that incorporates aluminum centers along with fumarate linkers, and is a promising material for applications involving adsorption of gases such as CO_2. In this work, the solvothermal synthesis and detailed characterization of the gallium and indium fumarate MOFs (Ga-fumarate, In-fumarate) are described. Using a combination of powder X-ray diffraction, Rietveld refinements, solid-state NMR spectroscopy, infrared spectroscopy, and thermogravimetric analysis, the topologies of Ga-fumarate and In-fumarate are revealed to be analogous to Al-fumarate. Ultra-wideline ^{69}Ga, ^{71}Ga and ^{115}In NMR experiments at 21.1 T strongly support our refined structure. Adsorption isotherms show that the Al-, Ga-, and In-fumarate MOFs all exhibit an affinity for CO_2, with Al-fumarate the superior adsorbent at 1 bar and 273 K. Static direct excitation and cross-polarized ^{13}C NMR experiments permit investigation of CO_2 adsorption locations, binding strengths, motional rates, and motional angles that are critical to increasing adsorption capacity and selectivity in these materials. Conducting the synthesis of the indium-based framework in methanol demonstrates a simple route to introduce porous hydrophobicity into a MIL-53-type framework, by incorporation of metal-bridging $–OCH_3$ groups in the MOF pores. ***Keywords:*** *metal organic frameworks, gas adsorption, X-ray diffraction, solid-state NMR, carbon dioxide, guest dynamics, porous hydrophobicity.*

Introduction

Metal-organic frameworks (MOFs) have been a topic of exceptional interest over the past twenty years due to their variety of useful properties and features such as high porosities, large surface areas, exceptional thermal stabilities, and significant catalytic activities.[1-2] MOFs are thus promising candidates for a wide range of applications[3] including gas storage,[4-6] gas separation,[5, 7-8] catalysis,[9-10] drug delivery,[11-12] and many others.[13-14]

The Al-fumarate MOF was first reported in a patent authored by BASF scientists[15] and has a low cost of production, good stability in water, and a relatively green synthetic route, which renders this MOF a promising candidate for applications in fields such as CH_4 and CO_2 capture and storage.[16] The structure of Al-fumarate was not initially solved, owing to the very small size of powdered product crystallites associated with the original synthetic route.[15, 17] A recent study showed that Al-fumarate is a structural analogue of the well-known MIL-53 MOF (Figure S1).[17]

Each Al metal center in Al-fumarate is coordinated to four oxygen atoms from four different fumarate ligands as well as two oxygen atoms from two separate bridging hydroxyl groups. The resulting AlO_6 building block is the fundamental octahedral secondary building unit (SBU) in Al-fumarate. A one-dimensional chain along the crystallographic *a*-axis is formed by corner-sharing SBUs connected *via* the bridging

hydroxyl groups; in turn, the chains along the *a*-axis are cross-linked by fumarate linkers to form rhombic-shaped channels.[17] The framework of Al-fumarate is rigid, thus there is only a small contraction of the unit cell after evacuating guest water molecules from the channels while the pore shape and dimensions are generally preserved.[17] In contrast, the structural analogue MIL-53 features 1,4-benzenedicarboxylate linkers, which imparts flexibility to MIL-53 and gives rise to an interesting "breathing effect:"[18-19] the dimensions of the channels can be altered by changing the nature and loading level of guest molecules.

Many properties and potential applications of the relatively new Al-fumarate MOF have not yet been explored, in contrast to the detailed studies and known applications for many other MOFs. There have been several adsorption isotherms reported for various gases in Al-fumarate;[17, 20-23] these include a report indicating that Al-fumarate is a promising CO_2 and H_2 storage material that exhibits good CO_2 selectivity for the separation of CO_2/CH_4 and CO_2/CO gases,[24] and also shows potential for the uptake of CO_2 in humid conditions.[21] Other recent reports indicate that Al-fumarate is a good material for fluoride uptake from water[25] as well as heat transformation,[26] and has possible applications for mechanical energy storage.[27] Previous studies have demonstrated that changing the metal center in a particular family of MOFs influences physical or chemical properties, such as gas adsorption affinity[4, 6] and catalytic activities.[28-29] It is highly likely that substituting another metal for the aluminum centers

within Al-fumarate will generate analogous MOFs that exhibit new or modified properties.

With the aims of expanding the fumarate MOF family and exploring their intriguing properties and applications, we (i) report a new synthetic route for obtaining the gallium-fumarate MOF, (ii) unambiguously characterize Ga-fumarate by a combination of X-ray diffraction and solid-state spectroscopy, showing that the structure is likely different from previously suggested,[30] and (iii) report the first synthesis and detailed examination of two different indium-fumarate MOFs, including one with porous hydrophobicity. Synchrotron powder X-ray diffraction (pXRD), Rietveld refinements, infrared spectroscopy (IR), multinuclear solid-state NMR spectroscopy, and thermogravimetric analysis (TGA) techniques have been employed to examine Ga-fumarate and In-fumarate from the perspective of both the host MOFs and guest CO_2 molecules. More specifically, we examine the CO_2 adsorption locations and the types of CO_2 motion present in Al-, Ga-, and In-fumarate, along with the parameters defining the motions associated with CO_2. Comprehensive combined characterization using the aforementioned techniques provides invaluable structural and dynamic information that points toward Al-, Ga-, and In-fumarate applications in areas such as selective adsorption. This work also describes a novel route to design hydrophobic MOFs, which are critically important for gas storage and separation in industrial applications.

Experimental

Synthesis of the Ga-fumarate MOF. In order to optimize the solvothermal synthesis of Ga-fumarate, the use of various gallium sources ($Ga(NO_3)_3 \cdot xH_2O$, $Ga_2(SO_4)_3 \cdot xH_2O$, Ga_2O_3), solvents *(N,N*-dimethylformamide (DMF), H_2O, methanol, ethanol, acetone, acetonitrile, tetrahydrofuran), temperatures (60 °C to 180 °C), and gallium salt/formate ligand ratios (1 : 1 and 1 : 2) was investigated. With these variables, Ga-fumarate could only be solvothermally synthesized in our laboratory using temperatures ranging from 60 °C to 180 °C, $Ga(NO_3)_3 \cdot xH_2O$ as the Ga source, and DMF as the solvent. The optimal temperature was found to be 80 °C and the ideal ratio of starting materials was determined to be 1:1, on the basis that these conditions yielded a Ga-fumarate product that exhibited the highest measured Brunauer–Emmett–Teller (BET) surface area of 851 m^2/g. Powder XRD patterns of the products that were obtained using different synthesis temperatures can be found in Figure S2.

The reagents $Ga(NO_3)_3 \cdot xH_2O$ (1.28 g, 5 mmol), fumaric acid ($C_4H_4O_4$, 0.58 g, 5 mmol), and DMF (10 mL) were mixed together in a 23 mL Teflon-lined stainless steel autoclave, which was then sealed and heated in an oven at 80 °C for 3 days. After letting the autoclave cool back to room temperature, the white product was obtained as a powder, which was washed three times with DMF and dried using vacuum filtration (elemental analysis (EA) of as-made Ga-fumarate: C: 27.51 %, N: 3.67 %, H: 3.43 %). The sample was then activated under dynamic vacuum for 8 h at a temperature of 150 °C in order to

evacuate residual unbound linker and solvent from the MOF channels.

We note that the synthesis of Ga-fumarate detailed in this work differs from the recently reported synthesis:[30] the solvent used here is DMF instead of water and NaOH.

Synthesis of the two In-fumarate MOFs. The synthesis of the In-fumarate MOF was performed using solvothermal techniques, and was optimized according to the synthetic conditions that resulted in the greatest BET surface area of the product. The variables investigated included solvents (DMF, H_2O, methanol, ethanol, acetone, acetonitrile, tetrahydrofuran), temperatures (20 °C to 140 °C), and indium salt/formate ligand ratios (1 : 1 and 1 : 2). It was found that In-fumarate could be solvothermally synthesized by using $In(NO_3)_3 \cdot xH_2O$ as the In source and either ethanol or methanol as the solvents, and by utilizing temperatures ranging from 20 °C to 120 °C (Figure S3 and Figure S4). The optimized syntheses are described below.

Hydrophilic In-fumarate (In-fumarate-E). $In(NO_3)_3 \cdot xH_2O$ (0.15 g, 0.5 mmol), fumaric acid ($C_4H_4O_4$, 0.116 g, 1.0 mmol), and ethanol (10 mL) were mixed together in a 20 mL glass vial, which was then sealed and heated at 40 °C for 3 days. The white product was obtained as a powder, which was washed three times with ethanol and dried using vacuum filtration (elemental analysis of as-made In-fumarate-E: C: 20.79 %, H: 1.99 %, N: not analyzed). The sample was then activated under dynamic vacuum for 8 h at a temperature of 150 °C to evacuate residual linker and solvent from the MOF channels.

The BET surface area of In-fumarate-E after activation was measured as 708 m^2/g.

Hydrophobic In-fumarate (In-fumarate-M). $In(NO_3)_3 \cdot xH_2O$ (0.15 g, 0.5 mmol), fumaric acid ($C_4H_4O_4$, 0.058 g, 0.5 mmol), and methanol (10 mL) were mixed together in a 20 mL glass vial, which was then sealed and left unagitated at 20 °C for 3 days. The product was obtained as a white powder, which was washed three times with methanol and dried using vacuum filtration (elemental analysis of as-made In-fumarate-M: C: 21.75 %, H: 1.70 %, N: not analyzed). The sample was then activated under dynamic vacuum for 8 h at a temperature of 150 °C in order to evacuate residual linker and solvent from the MOF channels. The BET surface area of In-fumarate-M after activation was 599 m^2/g.

All other experimental details concerning characterization can be found in the Supporting Information, including powder X-ray diffraction data, Rietveld refinement of the Ga fumarate MOF structure, BET surface area and CO_2 adsorption isotherm measurements, FT-IR spectroscopy, solid-state (^{13}C, ^{1}H, $^{69/71}Ga$, ^{115}In) NMR experiments, simulations, DFT calculations, TGA, SEM and elemental analysis.

Results and Discussion

Synthesis, characterization, and structural refinement of Ga-fumarate

It should be noted that during the preparation of this manuscript, another research group published a synthesis of the Ga-fumarate MOF;[30] however, their synthesis conditions were different, and there is good reason to believe our reported crystal structure more accurately describes the structure of Ga-fumarate. This is addressed in the following sections as appropriate.

Synthesis of Ga-fumarate. The solvothermal method with several different solvents was investigated as a route to synthesize Ga-fumarate. Only DMF solvent yielded a crystalline Ga-fumarate product with a pXRD pattern resembling that of Al-fumarate (*vide infra*). Methanol and ethanol solvents yielded crystalline powder products that did not exhibit the expected type of pXRD pattern, were not porous, and lost all crystallinity after attempting various activation strategies; these products will not be discussed any further. Amorphous products were obtained using H_2O, acetone, tetrahydrofuran and acetonitrile as solvents.

Our optimized solvothermal synthesis of Ga-fumarate in DMF requires heating a DMF solution of $Ga(NO_3)_3 \cdot xH_2O$ and fumaric acid in an autoclave at a temperature of 80 °C for 3 days, and then washing the white powdered product three times with DMF to obtain as-made Ga-fumarate (Ga-fumarate(*as*)) that contains DMF within the pores. A recently reported hydrothermal synthesis of Ga-fumarate employs water as the solvent, with NaOH, and a temperature of 130 °C;[30] the identical pXRD patterns of Ga-fumarate obtained using this method and our own indicate that these products are the same.

Powder XRD investigation of Ga-fumarate. Preliminary characterization of the various Ga-fumarate forms was performed using pXRD. The pXRD reflections of Ga-fumarate(*as*), which contains DMF, are positioned in the areas where one would expect to find the reflections of water-loaded Al-fumarate (Al-fumarate-H_2O, Figure 1). After activation to purge the MOF pores of DMF and residual fumarate linker, followed by exposure to ambient conditions to adsorb H_2O, Ga-fumarate(*as*) becomes Ga-fumarate-H_2O, which yields a pXRD pattern that is strikingly similar to that of Al-fumarate-H_2O and exhibits similar reflection angles and intensities (Figure 1); this data suggests Ga-fumarate and Al-fumarate reside in a similar crystal structure and space group. All of the Ga-fumarate-H_2O pXRD reflections are shifted to comparatively lower 2θ angles versus those of Al-fumarate-H_2O; this may reflect an enlarged *d*-spacing and slightly altered pore size in Ga-fumarate-H_2O due to the relatively larger Ga metal centers.

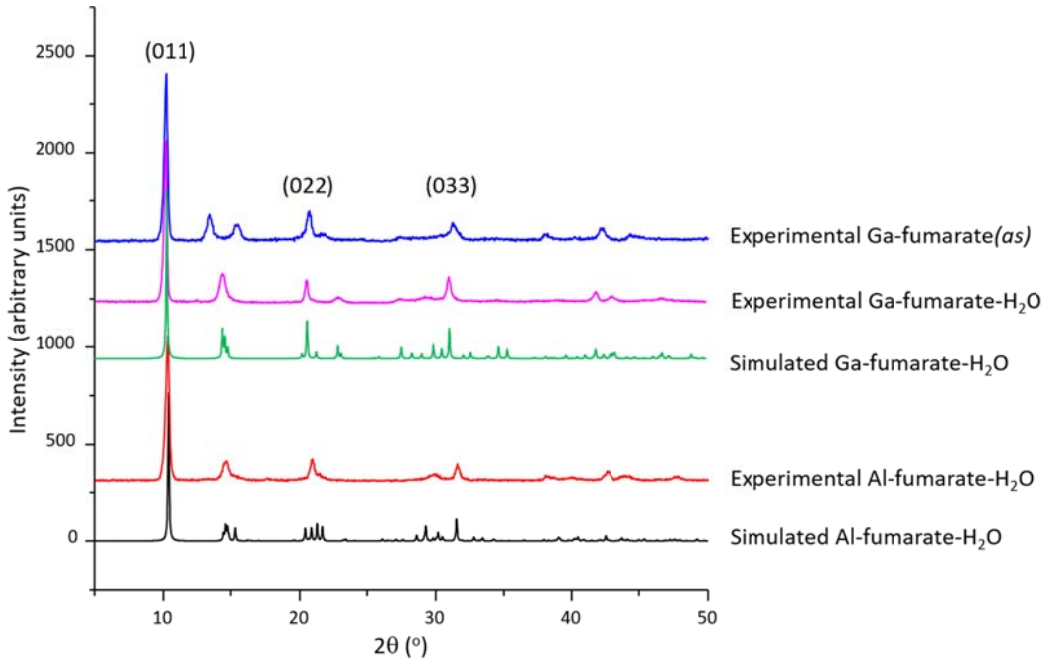

Figure 1. A comparison of simulated and experimental pXRD patterns of Al- and Ga-fumarate MOFs, with select reflections labeled. The samples with water adsorbed within the channels are termed Al-fumarate-H_2O and Ga-fumarate-H_2O, respectively. The as-made sample of Ga-fumarate is referred to Ga-fumarate(*as*). The 0kk reflections of Ga-fumarate-H_2O are shifted to lower angles versus those of Ga-fumarate(*as*), which indicates a small contraction of the MOF channel that propagates along the direction of the fumarate linker. Note the x-axis is truncated to exclude angles below 5 °.

The structural stability and rigidity of Ga-fumarate was also investigated. Activated Ga-fumarate was immersed in various solvents for 7 days, and then allowed to dry. The pXRD patterns after solvent exposure remain well-defined and are quite similar (Figure S5(a)). This result is a clear indication that Ga-fumarate is chemically robust, retaining its structure and high degree of crystallinity after solvent treatment. Powder XRD experiments were also used to compare Ga-fumarate to its structural analogue, the flexible MIL-53, which exhibits distinct pXRD patterns depending on the guest (i.e., DMF versus H_2O).[31-34] Our experimental pXRD patterns of Ga-fumarate(*as*) and Ga-fumarate-H_2O are generally similar (Figure 1), confirming that Ga-fumarate is rigid.

^{1}H NMR and IR spectroscopy. In order to perform accurate structural determination, the presence of key functional groups must typically be established. From Al-fumarate, it is known that there should be bridging –OH groups that join MO_6 (M: metal) SBUs in Ga-fumarate, which are very important functional groups that have been shown to act as guest (*i.e.*, CO_2) adsorption sites in MOFs such as the structurally similar MIL-53 system.[35-37] Prior to structural refinement, NMR and IR experiments were undertaken to determine if bridging -OH groups are present in Ga-fumarate.

The ^{1}H NMR spectra of Ga-fumarate feature a resonance located at ca. 2.6 ppm in activated Ga-fumarate (Figure 2(a)), which is assigned to bridging –OH groups joining GaO_6 SBUs; this resonance is proximate to that of bridging –OH groups in activated Al-fumarate (1.75 ppm),[17] with the slight divergence in chemical shifts due to the nature and influence of the different metal centers. The presence of a bridging –OH group is confirmed through the observation of an O-H stretching absorption at 3670 cm^{-1} in the IR spectrum of activated Ga-fumarate (Figure 2(b)), which is located in the expected region for bridging –OH groups in corner-sharing chains of metal-centered octahedra.[32] Additional results and discussion on ^{1}H NMR and IR experiments of Ga-fumarate(*as*) and Ga-fumarate-H_2O can be found in the Supporting Information. With knowledge of the linker structure, nature of the metal center, and presence of bridging –OH functional groups, the structure of Ga-fumarate could be solved.

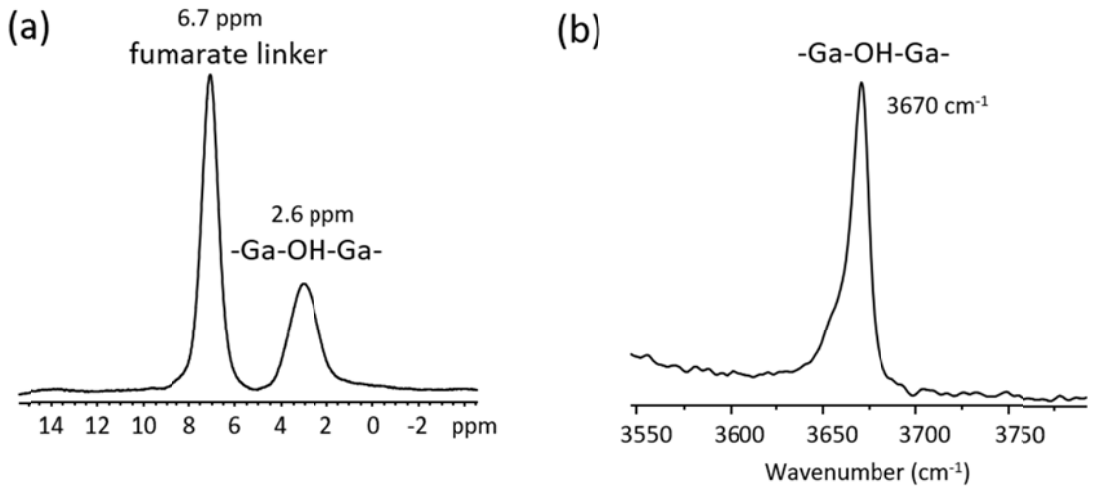

Figure 2. (a) The ^{1}H MAS NMR spectrum of activated Ga-fumarate, acquired at a spinning frequency of 14 kHz and a magnetic field of 9.4 T. The high-frequency resonance at 6.7 ppm corresponds to the hydrogen atom of the fumarate linkers, and the resonance at 2.6 ppm originates from the bridging hydroxyl groups that join the GaO_6 SBUs. In (b), the IR spectrum of activated Ga-fumarate is depicted; the absorption at 3670 cm^{-1} corresponds to the O-H stretch of the bridging hydroxyl groups.

Rietveld refinements of synchrotron X-ray diffraction data of Ga-fumarate. We were unable to obtain single crystals of sufficient size or quality for single-crystal XRD analysis, thus, Rietveld refinements of pXRD data were undertaken to determine the structure of Ga-fumarate. Activated Ga-fumarate readily adsorbs water from the air to become Ga-fumarate-H_2O with a formula of $Ga(OH)(C_4H_2O_4)\cdot 3.5H_2O$, where ($C_4H_2O_4$) represents the fumarate linker and the 3.5 H_2O/Ga ratio was determined from TGA (Figure S6). The pXRD pattern of Ga-fumarate-H_2O used for refinement was acquired using synchrotron radiation at the Canadian Light Source facility. As a starting point for the refinement, the previously determined structure of Al-fumarate-H_2O was used.[17]

The Rietveld refinement of Ga-fumarate-H_2O (Figure 3) yielded a monoclinic unit cell in the *I2/a* (no. 15) space group: a = 6.840(1) Å, b = 12.133 (2) Å, c = 12.315(2) Å, α =

γ = 90°, β = 94.85(2)°, V = 1018.4(3) Å^3. The goodness-of-fit parameters are χ^2 = 1.88, R_p = 3.8 %, and R_{wp} = 5.5 %. In contrast, a very recent work[30] reports a structure for the Ga-fumarate-H_2O framework in space group *P2$_1$/c*, leading to poor goodness-of-fit parameters χ^2 = 5.37, R_p = 9.22 %, and R_{wp} = 13.79 %, although it should be noted that only structure-less Le Bail refinement was performed in that case and the structure presented in this work is a DFT optimized structure. Refinement of the current data using the *P2$_1$/c* structure yielded an inferior fit and, importantly, the refinement would not converge, suggesting an issue with the *P2$_1$/c* model. Aside from the symmetry change, there are minor differences between the two structures. The carboxylate groups on the fumarate linkers are closer to planar in the *I2/a* structure compared to the *P21/c* structure, which exhibits carboxylate groups with larger torsion angles relative to the fumarate backbone. The distribution of water molecules in the pores is also different; the *P2$_1$/c* structure has four symmetry-independent water molecules while the *I2/a* structure has only two. Detailed comparison of the hydrogen bonding is difficult given hydrogen coordinates on the water molecules could not be determined with the current experimentally refined *I2/a* structure. Based on the above discussion, we believe that space group *I2/a* better represents the crystal structure of Ga-fumarate-H_2O. Strong evidence for the *I2/a* space group is also provided by ^{69}Ga and ^{71}Ga NMR spectra along with DFT calculations (*vide infra*).

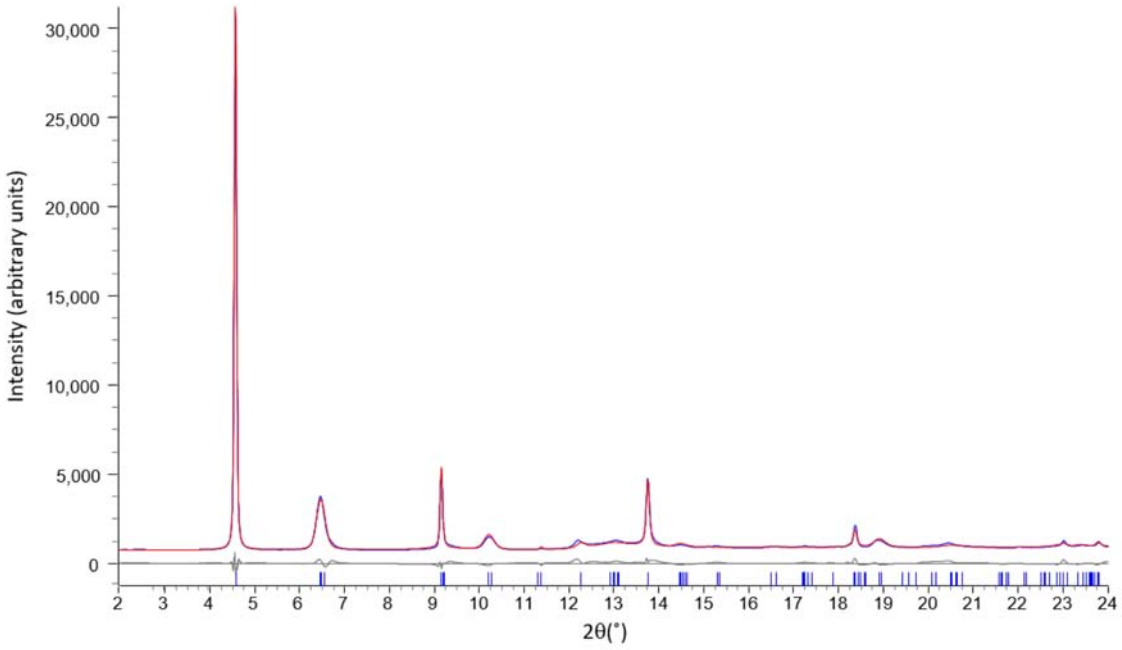

Figure 3. The calculated Rietveld plot of Ga-fumarate-H_2O is shown in blue, along with the experimental synchrotron pXRD pattern in red and a difference plot below in green. The associated goodness-of-fit parameters are $\chi^2 = 1.88$, $R_p = 3.8$ %, and $R_{wp} = 5.5$ %.

The refined structure of Ga-fumarate-H_2O features a single crystallographically unique Ga site. In terms of connectivity and topology, the structures of Ga-fumarate and Al-fumarate are similar. Ga is connected to six oxygen atoms to form a GaO_6 SBU (Figure 4(a)), where four oxygens are from fumarate linkers while the other two are from bridging hydroxyl groups connecting SBUs to form a one-dimensional chain (Figure 4(b)). The chains of SBUs are joined by fumarate linkers to form the long-range MOF structure, which features one-dimensional rhombic-shaped channels (Figure 4(c)) that measure *ca.* 12 x 12 Å from corner to corner. The pore sizes of Ga-fumarate-H_2O and Al-fumarate-H_2O are very proximate,[17] in line with the numerous structural similarities between the two

MOFs. As expected, the Ga-fumarate-H_2O channels are occupied by guest H_2O molecules adsorbed from air; only the oxygen positions of H_2O could be refined, with the result depicted in Figure 4(d). The shortest distance between the oxygen atoms of water molecules (O_w) and the hydrogen atoms of bridging –OH groups in Ga-fumarate-H_2O is 2.488 Å, indicating there may be an interaction between the two.

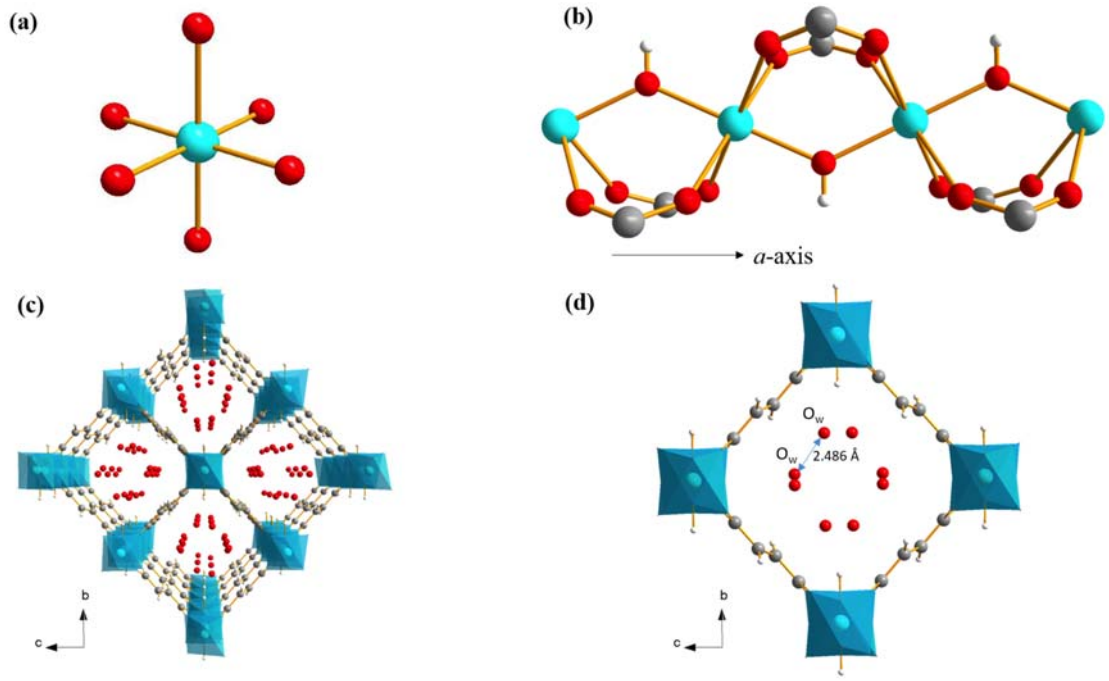

Figure 4. The local and long range structure of Ga-fumarate-H_2O. In (a), the GaO_6 octahedral environment associated with the $GaO_4(OH)_2$ secondary building unit (SBU) is shown. The SBUs are linked by bridging hydroxyl (OH) groups to form a chain of SBUs along the crystallographic *b*-axis, as shown in (b). The SBU chains are interconnected by fumarate linkers to create the one-dimensional rhombic channels illustrated in (c). The oxygen atoms associated with water molecules in the channels are depicted more clearly in (d). The colors red, grey, white and blue correspond to oxygen, carbon, hydrogen and the gallium metal center, respectively

$^{69/71}$Ga NMR experiments at 21.1 T. Solid-state NMR of metal centers in MOFs can be a source of rich structural information.[38] In this instance, there is an inherent

difficulty with performing ^{69}Ga and ^{71}Ga NMR experiments due to the quadrupolar nature of these spin 3/2 nuclei; ^{69}Ga and ^{71}Ga possess large quadrupole moments of 171 and 107 mb, respectively.[39] These large quadrupole moments couple with surrounding EFGs in a process known as the quadrupolar interaction (QI), which often spreads the ^{69}Ga and ^{71}Ga central transition (i.e., spin -1/2 $\leftrightarrow$ +1/2) resonance across large frequency ranges, yielding very broad powder patterns of low signal-to-noise ratio (S/N). The chemical shift (CS) interaction also has a very minor influence on ^{69}Ga and ^{71}Ga spectra. NMR parameters relating to the CS and QI are described in more detail within the Supporting Information.

^{69}Ga and ^{71}Ga NMR spectra of MOFs such as MIL-53, MIL-61, MIL-96, MIL-120 and MIL-124 have been reported.[40-41] In this study, we have used NMR experiments at a magnetic field of 21.1 T to acquire ^{69}Ga and ^{71}Ga spectra of activated Ga-fumarate and Ga-fumarate-H_2O. Acquisition of both ^{69}Ga and ^{71}Ga spectra permits accurate determination of NMR parameters.

The experimental and simulated ^{69}Ga and ^{71}Ga NMR spectra of activated Ga-fumarate and Ga-fumarate-H_2O are shown in Figure 5, and all NMR parameters are listed in Table S1. The ^{71}Ga NMR spectra (Figure 5(a)) are narrower than their ^{69}Ga counterparts (Figure 5(b)), owing to the larger quadrupole moment of ^{69}Ga. The relatively lower simulated versus experimental intensity of the low-frequency “horn” of all ^{71}Ga spectra and in the ^{69}Ga spectrum of Ga-fumarate-H_2O is likely due to anisotropic

T_2 relaxation (Figure S14), which has been observed for spin-1/2 and quadrupolar nuclei in a variety of systems.[42-43]

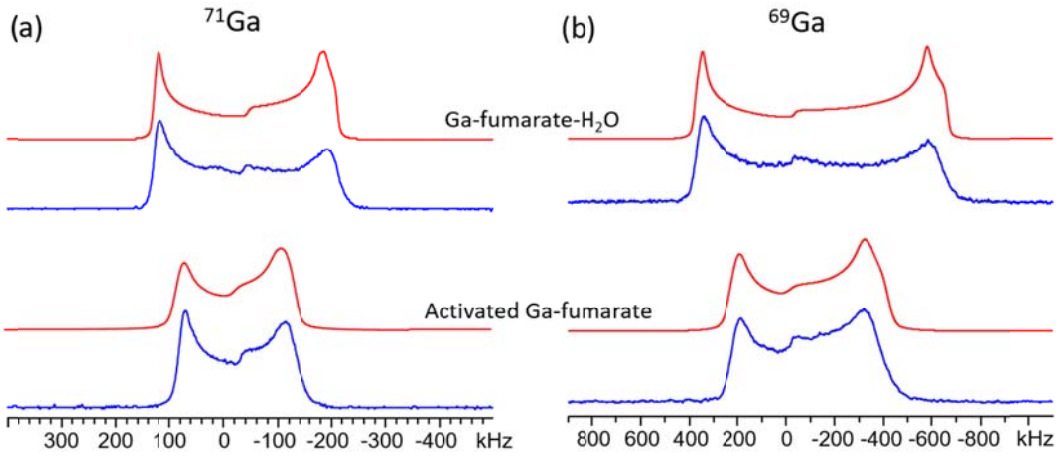

Figure 5. Static ^{69}Ga and ^{71}Ga NMR spectra acquired at 21.1 T. In (a), the experimental ^{71}Ga NMR spectra of Ga-fumarate-H_2O and activated Ga-fumarate are shown in blue, along with simulations of the experimental spectra in red. The corresponding ^{69}Ga NMR spectra in blue and simulations of the same compounds in red are given in (b).

The ^{69}Ga and ^{71}Ga NMR spectra of activated Ga-fumarate and Ga-fumarate-H_2O are characteristic of a quadrupolar nucleus residing in one unique local environment. The single Ga site observed in NMR experiments is in agreement with the one crystallographically unique Ga indicated from our refined structure of Ga-fumarate-H_2O, and stands in contrast to the four unique Ga sites proposed in a recent structural model.[30] The ^{69}Ga and ^{71}Ga powder patterns of Ga-fumarate-H_2O are significantly broader than those of activated Ga-fumarate (Figure 5) and correspond to higher C_Q values (Table S1), indicating that a reduction of spherical symmetry about Ga occurs during the hydration process. From these observations, it is apparent that H_2O within the channels of Ga-fumarate-H_2O must be influencing the Ga local environment by

either (i) directly influencing the EFG at Ga (*i.e.*, very close proximity or bonding to Ga), or (ii) interacting with the linkers or bridging hydroxyl groups between GaO_6 SBUs, which subsequently distorts the GaO_6 SBUs and modifies the EFG at Ga. The ^{69}Ga and ^{71}Ga EFG asymmetry parameter (η_Q) of both hydrated (η_Q = 0.09) and dehydrated (η_Q = 0.13) Ga-fumarate reflect a high degree of axial symmetry that is not significantly altered by hydration. The very similar η_Q values suggest that no H_2O-Ga bonds are formed during the hydration of Ga-fumarate, since any additional bonding would significantly impact n_Q. In summary, the changes in C_Q(^{69}Ga, ^{71}Ga) with hydration of Ga-fumarate along with stationary n_Q values are likely due to variations in Ga-O bond lengths or ∠O-Ga-O bond angles that originate from relatively strong H_2O interactions with the bridging hydroxyl groups joining GaO_6 octahedra.

Plane-wave DFT calculations of ^{69}Ga and ^{71}Ga EFG tensor parameters were performed on the geometry-optimized structures of activated Ga-fumarate and Ga-fumarate-H_2O (Table S1). Since only the Ga-fumarate-H_2O structure was solved via Rietveld refinements, the crystal structure of activated Ga-fumarate was constructed by removing water molecules from the channels of the refined Ga-fumarate-H_2O structure, followed by a plane-wave DFT geometry optimization. All geometry optimization calculations were performed with symmetry constrained to the *I2/a* space group. After geometry optimization, both the activated Ga-fumarate and Ga-fumarate-H_2O structures feature a single crystallographically unique Ga site (Table S1), which is consistent with

^{69}Ga and ^{71}Ga NMR results. The calculated C_Q(^{69}Ga, ^{71}Ga) and η_Q values of activated Ga-fumarate and Ga-fumarate-H_2O are in good agreement with experimental values (Table S1). The calculated C_Q(^{69}Ga, ^{71}Ga) values in Ga-fumarate-H_2O slightly underestimate the observed C_Q(^{69}Ga, ^{71}Ga) values, likely because the DFT calculations assume a static arrangement of water molecules at well-defined positions within the channels. ^{69}Ga and ^{71}Ga NMR experiments were performed at room temperature; under these conditions the water molecules are disordered and dynamic, allowing H_2O to sample space proximate to the Ga center and/or interact with the linkers bound to Ga, reducing the spherical symmetry of GaO_6 SBUs within Ga-fumarate-H_2O and increasing experimental C_Q(^{69}Ga, ^{71}Ga) values.

Plane-wave DFT calculated $^{69/71}$Ga NMR parameters based on the published Ga-fumarate-H_2O structure (space group: *P2$_1$/c*) significantly deviate from the experimental value and incorrectly indicate that four Ga sites are present, while calculations using the *I2/a* Ga-fumarate-H_2O structure reported in this work produce a single set of $^{69/71}$Ga NMR parameters that are much closer to the observed NMR parameters from the sole unique Ga site (Table S1). A comparison of calculated spectra obtained from these two structures and space groups is shown in Figure S15, which again supports the *I2/a* space group. In summary, the results from PXRD refinements, $^{69/71}$Ga NMR experiments and DFT calculations are consistent with Ga-fumarate-H_2O crystallizing in a space group of *I2/a* with only a single Ga site in the unit cell.

Synthesis and characterization of In-fumarate

We found that pure, crystalline In-fumarate MOFs could be synthesized solvothermally using either methanol or ethanol as the solvent. The synthesis of In-fumarate requires remarkably little thermal energy, with optimized syntheses using ethanol and methanol requiring temperatures of only 40 °C and 20 °C, respectively. The hydrophilicity and hydrophobicity of In-fumarate can be tuned through the use of a particular solvent: ethanol yields hydrophilic In-fumarate (In-fumarate-E), while methanol leads to hydrophobic In-fumarate (In-fumarate-M).

Hydrophilic In-fumarate-E

TGA indicates In-fumarate-E could adsorb water vapor from the air. The pXRD patterns of In-fumarate-E are shown in Figure 6. The experimental pXRD pattern of as-made In-fumarate-E (In-fumarate-E(*as*)) material strongly resembles the simulated and experimental pXRD patterns for the Ga-fumarate-H_2O framework, indicating that their respective structures are very similar. The pXRD pattern of In-fumarate-E-H_2O material obtained after evacuation followed by adsorption of water is nearly identical to that of In-fumarate-E(*as*), indicating that In-fumarate-E also exhibits a remarkably rigid framework. The pXRD reflections of all In-fumarate-E samples are shifted to lower 2θ-angles versus those of the corresponding Ga-fumarate framework, most likely due to the relatively larger size of In metal centers and corresponding slight difference in pore

size.

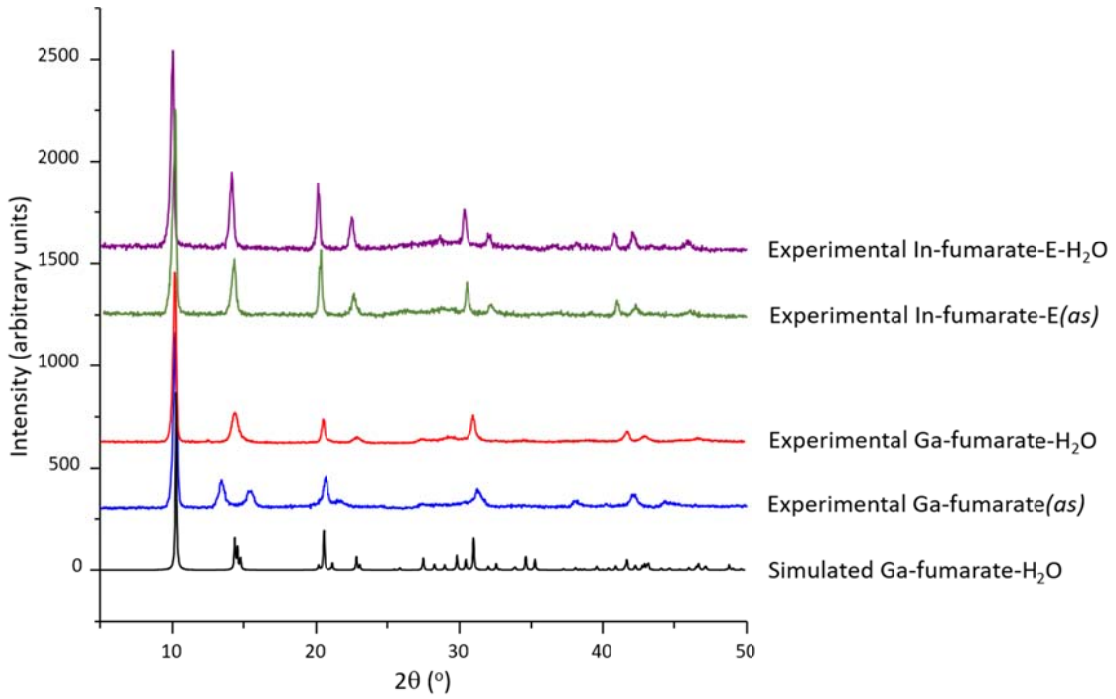

Figure 6. A comparison of simulated and experimental pXRD patterns of Ga-fumarate and experimental pXRD patterns of In-fumarate-E. The samples with water inside the channels are termed Ga-fumarate-H_2O and In-fumarate-E-H_2O, respectively. The as-made samples of Ga-fumarate and In-fumarate-E are referred to Ga-fumarate(*as*) and In-fumarate-E*(as)*.

The presence of bridging –OH groups joining InO_6 SBUs within the In-fumarate-E framework was confirmed *via* ^{1}H MAS NMR and IR spectroscopy. The ^{1}H MAS NMR spectrum of activated In-fumarate-E features a resonance at ca. 1.9 ppm (Figure 7(a)) that is assigned to bridging –OH groups. The IR spectrum of activated In-fumarate-E has an O-H stretching absorption at 3666 cm^{-1} (Figure 7(b)) that is assigned to bridging -OH groups. Additional IR spectra as well as ^{1}H MAS and ^{1}H-^{13}C CP/MAS NMR spectra of various In-fumarate-E forms can be found in the Supporting Information.

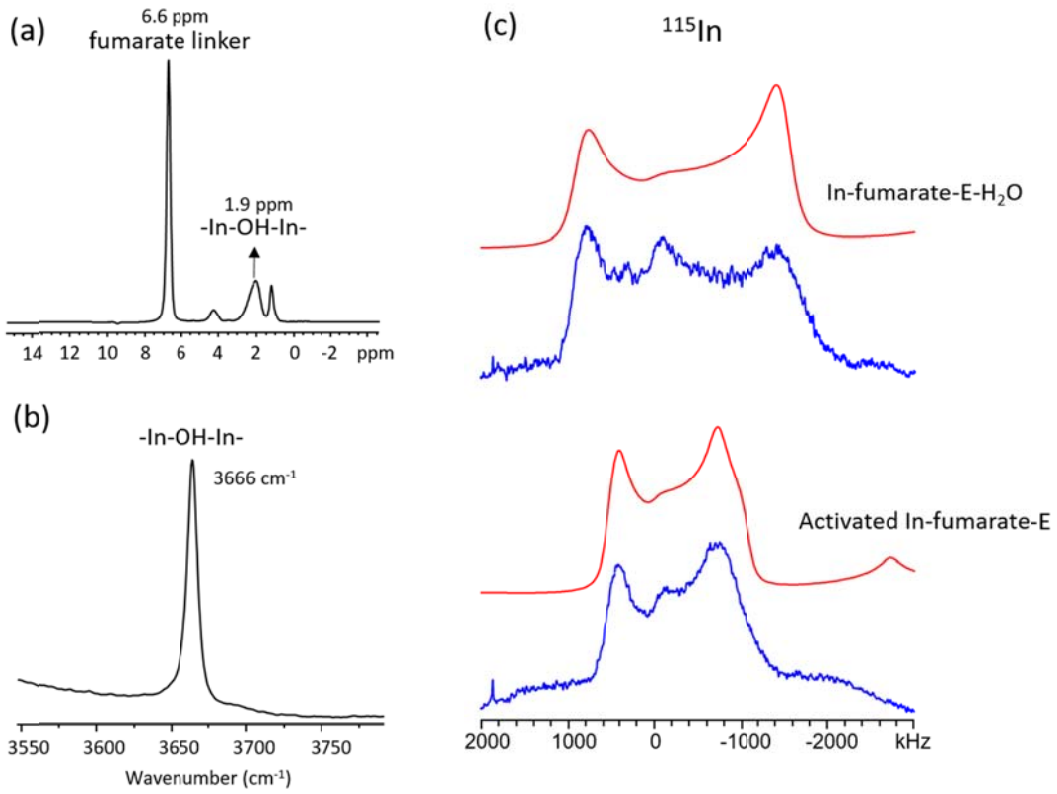

Figure 7. The ^{1}H MAS NMR spectrum of activated In-fumarate-E, as acquired using a spinning frequency of 31.25 kHz and magnetic field of 21.1 T, is shown in (a). The detailed assignments for each resonance in (a) can be found in Figure S10. The IR spectrum of activated In-fumarate-E is depicted in (b); the absorption at 3666 cm^{-1} corresponds to the O-H stretch of the bridging hydroxyl groups. The experimental (blue) and simulated (red) ^{115}In NMR spectra of In-fumarate-E-H_2O and activated In-fumarate-E at 21.1 T are shown in (c). The additional spectral intensity on either side of the powder pattern arises from ^{115}In satellite transitions.

^{115}In NMR experiments at 21.1 T were performed on In-fumarate-E to probe the local metal environment. ^{115}In is considered to be a very challenging nucleus for NMR study due to its very large quadrupole moment of 770 mb,[39] which leads to extremely broad powder patterns of low S/N in environments of low symmetry. A variety of materials have been studied *via* ^{115}In NMR spectroscopy,[44-47] however to the best of our knowledge, ^{115}In spectra have only been reported for the $In(BDC)_{1.5}(bipy)$, $In(BTC)(H_2O)(phen)$, and MIL-68 MOFs.[48-49]

The experimental and simulated static ^{115}In NMR spectra of activated In-fumarate-E and water adsorbed In-fumarate-E-H_2O are shown in Figure 7(c), with the corresponding ^{115}In NMR parameters contained in Table S2. Both MOFs yield a single ^{115}In NMR powder pattern, indicating that one crystallographically unique In site is present. The ^{115}In NMR spectrum of hydrated In-fumarate-E-H_2O is broader than that of dehydrated activated In-fumarate-E. Simulations of the activated In-fumarate-E ^{115}In NMR spectrum yield $C_Q(^{115}In)$ = 193(2) MHz and η_Q = 0.22(2), while In-fumarate-E-H_2O corresponds to $C_Q(^{115}In)$ = 260(3) MHz and η_Q = 0.00(2). Interactions between water molecules and the In-fumarate-E-H_2O framework modify the already uneven distribution of In-O bond lengths and/or ∠O-In-O bond angles within InO_6 SBUs, reducing their spherical symmetry and increasing $C_Q(^{115}In)$. The low η_Q values indicate that the InO_6 SBUs have a high degree of axial symmetry, while the reduced η_Q value in In-fumarate-E-H_2O is likely due to a slight distortion in the InO_6 octahedral geometry changing arising from interactions between water molecules and the framework.

Hydrophobic In-fumarate-M. One limitation for MOFs in industrial applications is water affinity, which may lead to mechanical and chemical instability.[50] For example, MOFs in gas capture applications can be degraded by or preferentially adsorb water molecules in the flue gas.[51] In this sense, the development of hydrophobic MOFs to avoid the detrimental effects of water is quite important. However, it should be noted that there are many known water stable MOFs, including those resistant or immune to

the effects of aqueous acids and bases.[52] Depending on the intended purpose and conditions, a hydrophilic, hydrophobic, or other type of MOF may be useful to address one of many industrial applications.[53]

We have synthesized hydrophobic In-fumarate (In-fumarate-M) by using methanol as the solvent. In-fumarate-M and In-fumarate-E share nearly identical pXRD patterns (Figure S16), indicating the two frameworks have the same topology. TGA performed on a sample of In-fumarate-M material after activation and exposure to 20% relative humidity for one week indicated the absence of any adsorbed water (Figure 8(a)), with the only observed weight loss step taking place at ca. 400 °C, corresponding to MOF decomposition. Further ^{1}H MAS NMR (Figure S17) and TGA studies (Figure S18) on In-fumarate-M demonstrated that water adsorption only occurs under conditions of very high humidity (e.g. 80 %). The ^{13}C CP/MAS NMR spectrum of as-made In-fumarate-M contains two distinct ^{13}C resonances at 50.4 ppm and 53.4 ppm (Figure 8(b)), in a region where –OCH_3 resonances are typically found. The ^{13}C resonance at 50.4 ppm is removed by sample activation; this resonance is thus assigned to methanol molecules in the as-made sample. The other ^{13}C resonance at 53.4 ppm persists after activation and is slightly shifted to 53.0 ppm (Figure 8(c)). The spectroscopically determined presence of a hydrophobic –OCH_3 group within the In-fumarate-M MOF provides an explanation for its observed hydrophobicity.

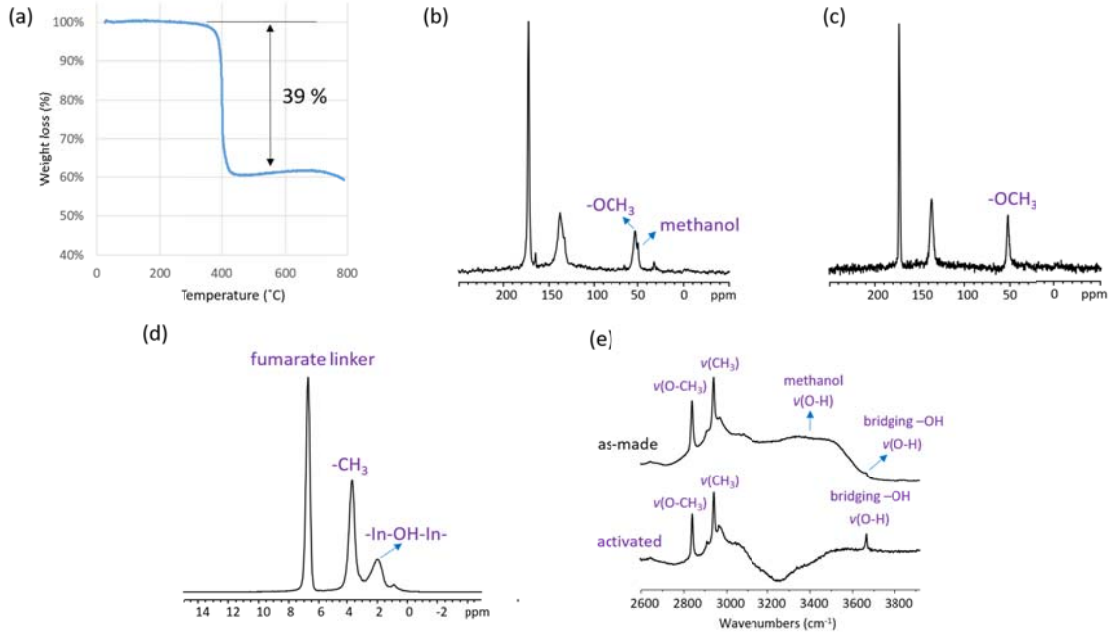

Figure 8. The spectral characterization of hydrophobic In-fumarate-M. A TGA plot of activated In-fumarate-M after exposure to air (20 % r.h.) for 7 days is illustrated in (a). The ^{13}C CP/MAS NMR spectra of as-made and activated In-fumarate-M are shown in (b) and (c), respectively. The ^{1}H MAS NMR spectrum of activated In-fumarate-M is illustrated in (d). The ^{13}C CP/MAS NMR spectra were acquired at magnetic field of 9.4 T using a spinning frequency of 14 kHz, while the ^{1}H MAS NMR spectrum was acquired at magnetic field of 21.1 T with a spinning frequency of 31.25 kHz. The IR spectra of as-made and activated In-fumarate-M are shown in (e).

The ^{115}In NMR powder pattern of In-fumarate-M activated and exposed to air for 7 days is very similar to those of activated In-fumarate-M and activated In-fumarate-E (Figure S19), with all C_Q and η_Q values within experimental uncertainties (Table S2). The indium metal centers within In-fumarate-M and In-fumarate-E materials thus reside in nearly identical local environments, indicating that the –CH_3 group within In-fumarate-M must not be directly bound to the metal center (see below). The ^{1}H MAS NMR spectrum of activated In-fumarate-M (Figure 8(d)) features a resonance at 3.6 ppm that is assigned to the –OCH_3 group within the framework, and the ^{1}H resonance on the hydroxyl group

of methanol cannot be detected. The IR spectrum again confirms that all methanol is indeed removed after activation, with the elimination of a strong and broad O-H methanol stretching adsorption between 3200 to 3600 cm^{-1} (Figure 8(e) and S12(e)). There is a clear O-CH_3 stretching adsorption at 2841 cm^{-1} in the IR spectrum of activated In-fumarate-M (Figure 8(e)), which is assigned to the new -OCH_3 group within the framework.[54] The O-H stretching band of bridging –OH in In-fumarate-M at 3666 cm^{-1} has a much lower intensity than that of In-fumarate-E (Figure S12 (d) and (e)), suggesting that there are relatively very few bridging –OH groups in this MOF.

Given the ^{1}H, ^{13}C, and ^{115}In NMR results, along with TGA and IR spectra, it appears that a –OCH_3 group replaces the bridging –OH group between InO_6 SBUs in In-fumarate-M, introducing hydrophobicity to this framework. Previous studies have shown that framework hydrophobicity in the structurally similar MIL-53 MOF can be enhanced by replacing the bridging hydroxyl group with alternate atoms.[55-57] In addition, post-synthetic exchange of both the linkers and cations is possible in MIL-53,[58] thus substitution of the –OH linker with –OCH_3 in the similar In-fumarate-M is within reason. To the best of our knowledge, the herein observed modification of In-fumarate-M represents the first reported strategy for introducing hydrophobic channels into a MIL-53-like MOF by incorporation of metal-bridging –OCH_3 groups into the framework, and also provides In-fumarate-M as the first example of a hydrophobic fumarate MOF.

Porosity and gas adsorption of Ga-fumarate and In-fumarate

BET surface area measurements. The measured BET surface areas of Ga-fumarate, In-fumarate-E, In-fumarate-M, and Al-fumarate were determined by measuring the N_2 adsorption isotherm at 77 K (Figure 9(a)). The Ga-fumarate sample synthesized at a temperature of 80 °C exhibited the highest BET surface area among all Ga-fumarate products at 851 m^2/g. Other synthesis temperatures yielded Ga-fumarate products with lower BET surface areas (Table S3). The 851 m^2/g BET surface area of Ga-fumarate is somewhat lower than the 1080 m^2/g value for Al-fumarate,[17] which is likely due to the higher atomic mass of Ga. The highest BET surface area of In-fumarate-E is 708 m^2/g, obtained from a sample synthesized at 40 °C (Table S4), while the highest BET surface area of In-fumarate-M is 599 m^2/g, as measured from a room temperature synthesis at 20 °C. The reduced BET surface area of In-fumarate-M as compared to In-fumarate-E is likely due to the replacement of bridging -OH groups to bulkier bridging -OCH_3 groups. It should be stressed that all these fumarate MOFs still exhibit very good BET surface areas with respect to porous materials in general.

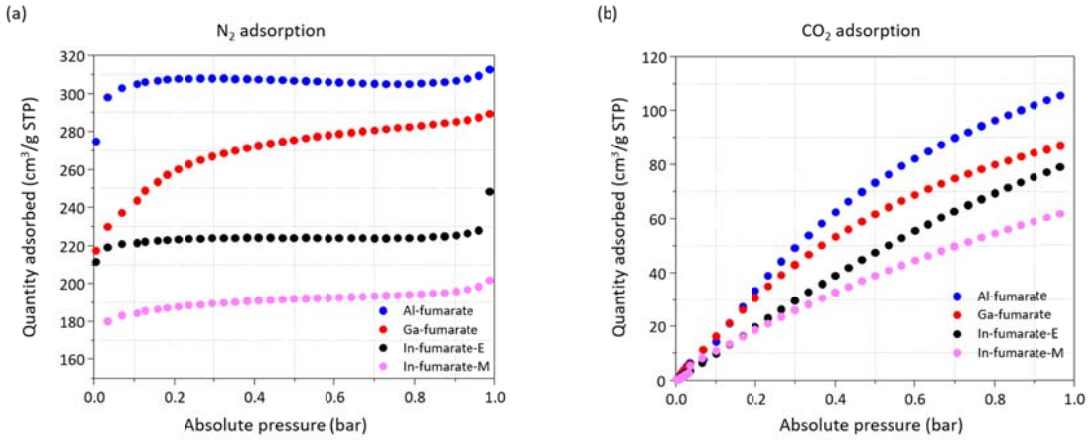

Figure 9. The N_2 adsorption isotherms of Al-fumarate, Ga-fumarate, In-fumarate-E, and In-fumarate-M are shown in (a), as measured at 77 K. In (b), the CO_2 adsorption isotherms of Al-fumarate, Ga-fumarate, In-fumarate-E, and In-fumarate-M at 273 K are illustrated.

CO_2 adsorption isotherm measurements. The CO_2 adsorption ability of Ga-fumarate, In-fumarate-E, and In-fumarate-M were determined by measuring the CO_2 adsorption isotherm at 273 K and comparing it to that of Al-fumarate (Figure 9(b)). At a pressure of 1 bar, Al-fumarate can adsorb 108 cm^3/g STP of CO_2, while Ga-fumarate adsorbs ca. 20 % less (88 cm^3/g STP). The In-fumarate-E and In-fumarate-M MOFs also have relatively lower CO_2 capacities of 81 cm^3/g STP and 62 cm^3/g STP, respectively. The lower CO_2 adsorption capacity in Ga-fumarate and In-fumarate is likely connected to their lower BET surface areas versus Al-fumarate; the decrease in CO_2 uptake along the group Al > Ga > In within this series of fumarate MOFs seems to be linked to an increase in MOF weight as heavier metal centers are incorporated. However, the relatively lower CO_2 capacities in the Ga-fumarate and In-fumarate MOFs may also be due to a relatively weaker CO_2 binding strength in these MOFs. The low CO_2 capacity within In-fumarate-M is likely also related to the presence of bridging $–OCH_3$ groups, which have replaced

bridging –OH groups, which are known to be the CO_2 adsorption sites in the structurally similar MIL-53 MOF.[35]

Static ^{1}H-^{13}C CP NMR experiments of CO_2 in ordinary and deuterated samples. Our prior work on MIL-53 MOFs has demonstrated that static ^{1}H-^{13}C CP NMR experiments at low temperatures, in conjunction with deuteration techniques, can be used to confirm if a MOF hydroxyl group serves as a CO_2 adsorption site.[35]

Both fumarate MOFs in this study possess a similar structure to MIL-53, where the MO_6 (M = Al, Ga, In) SBUs are connected through bridging hydroxyl groups, leading to the preliminary hypothesis that the CO_2 adsorption sites in Al-, Ga-, and In-fumarate are also located near the bridging hydroxyl groups. In order to verify this hypothesis, static ^{1}H-^{13}C CP NMR experiments were performed on (i) the empty frameworks, (ii) CO_2 loaded but non-deuterated fumarate MOFs featuring $–O^{1}H$ bridging hydroxyl groups, as well as (iii) CO_2 loaded and deuterated fumarate MOFs with $–O^{2}H$ groups.

The static ^{1}H-^{13}C CP NMR spectra of Al-fumarate samples acquired at 133 K with a contact time (CT) of 10 ms are shown in Figure 10(a). The broad, overlapping ^{13}C powder patterns observed in the empty framework arise solely from the carbon atoms of the fumarate linkers. The spectrum of CO_2 loaded non-deuterated Al-fumarate is similar to that of empty Al-fumarate, however, a small additional resonance at ca. 145 ppm (denoted * in Figure 10(a)) is apparent. This resonance is located at approximately the

same frequency as the overlapping δ_{11} and δ_{22} components of the ^{13}C CS tensor from adsorbed CO_2 (ca. 144 ppm at 133 K, Figure 11(a)), and represents adsorbed CO_2. The assignment of this resonance is unambiguous, since it is not apparent in the ^{1}H-^{13}C CP NMR spectrum of the CO_2 loaded deuterated Al-fumarate sample, which features a $-O^{2}H$ bridging hydroxyl group rather than a $-O^{1}H$ one. The static ^{1}H-^{13}C CP spectra indicate that the CO_2 adsorption site in Al-fumarate is on or near the bridging hydroxyl group.

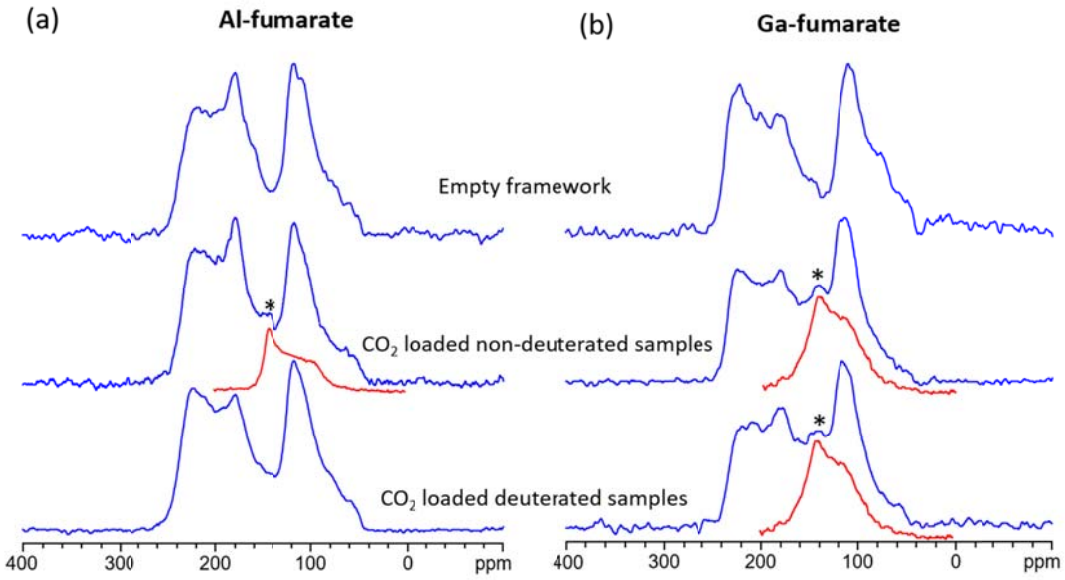

Figure 10. Static ^{1}H-^{13}C CP NMR spectra of (a) Al-fumarate and (b) Ga-fumarate acquired using a CP contact time of 10 ms at a temperature of 133 K are shown. The asterisk sign (*) denotes the ^{13}C resonance corresponding to adsorbed CO_2. In this Figure, all spectra colored in red correspond to the static ^{13}C DEPTH-echo NMR spectra of adsorbed $^{13}CO_2$ at 133 K.

The case of Ga-fumarate is quite different than that of Al-fumarate. ^{1}H-^{13}C CP NMR experiments on CO_2 loaded non-deuterated and deuterated Ga-fumarate samples give rise to very similar spectra (Figure 10(b)). There is a CO_2 resonance at ca. 143 ppm (denoted by the asterisk (*) and by the red spectra in Figure 10(b)) that is not present in

the empty framework CP spectrum, but is present in CP spectra of both the non-deuterated and deuterated fumarate MOF samples, indicating that ^{1}H-^{13}C CP to $^{13}CO_2$ is efficient, and thus CO_2 must be located near one or more ^{1}H atoms. Since the hydrogen atoms on the bridging hydroxyl groups have been replaced by deuterium atoms in deuterated Ga-fumarate, CO_2 must be interacting or proximate to hydrogen atoms on the organic fumarate linkers, which are not replaced during the deuteration process. Hence, despite the structural similarities between Al- and Ga-fumarate MOFs, the adsorption site is located near the bridging hydroxyl groups in Al-fumarate, while CO_2 adsorption must occur relatively closer to the fumarate linkers in Ga-fumarate.

The CO_2 resonance within CO_2-loaded non-deuterated In-fumarate-E and In-fumarate-M CP spectra (Figure S22) could not be observed due to the weaker CO_2 binding strength, therefore, it was not possible to locate the CO_2 adsorption sites within In-fumarate using ^{1}H-^{13}C CP NMR experiments.

^{13}C NMR targeting adsorbed $^{13}CO_2$ (0.2 CO_2/metal center). ^{13}C NMR experiments have been used to investigate CO_2 locations, dynamics, and relative binding strengths within MOFs.[35, 38, 59-73] In this work, we acquired static VT ^{13}C NMR spectra of CO_2-loaded Al-fumarate at temperatures ranging from 133 K to 373 K (Figure 11(a)), and those of CO_2-loaded Ga-fumarate, In-fumarate-E, and In-fumarate-M were acquired at temperatures between 133 K to 293 K (Figure 11(b), (c), (d)); the extracted CS parameters are summarized in Table S7. At 293 K, the static ^{13}C NMR spectra of $^{13}CO_2$

adsorbed in Al-fumarate features a powder pattern corresponding to a span (Ω) of 27(1) ppm and a skew (κ) value equal to +1. The observation of an anisotropic ^{13}C CS powder pattern, rather than a sharp isotropic resonance, confirms that CO_2 guests are participating in well-defined motions within Al-fumarate instead of rapid isotropic tumbling through the MOF. The apparent ^{13}C Ω value of CO_2 in Al-fumarate increases from 26(1) ppm at 373 K to 62(1) ppm at 133 K, while the observed κ value remains +1 throughout. It should be noted that the experimental CO_2 ^{13}C Ω value of 62 ppm at 133 K remains far smaller than the 335 ppm of static CO_2 at ca. 20 K,[74] indicating that CO_2 motion is present and partially removing the CS anisotropy. Furthermore, the continuous evolution of the ^{13}C powder pattern with temperature (*i.e.*, changes in Ω) is a clear indication that the experimental temperature influences the CO_2 motional angles, which in turn affect the ^{13}C NMR spectral appearance and the observed or apparent NMR parameters. At temperatures $\geq$ 313 K, an additional sharp resonance around 125 ppm originates from gaseous, unbound CO_2.[74]

The ^{13}C NMR spectra of $^{13}CO_2$ adsorbed in Ga-fumarate at 293 K consist of a single sharp isotropic resonance located at ca. 125 ppm (Figure 11(b)) with a full width at half height (FWHH) of 443 Hz. The narrow, featureless resonance indicates that CO_2 guests undergo very fast isotropic tumbling at 293 K, which removes the anisotropy (*i.e.*, spectral broadening effects) of the CS tensor. In contrast to the relatively broad ^{13}C powder pattern at 293 K in Al-fumarate, the rapid isotropic motion of CO_2 in

Ga-fumarate and narrow isotropic resonance indicates that CO_2 is bound relatively weaker to the Ga analogue.

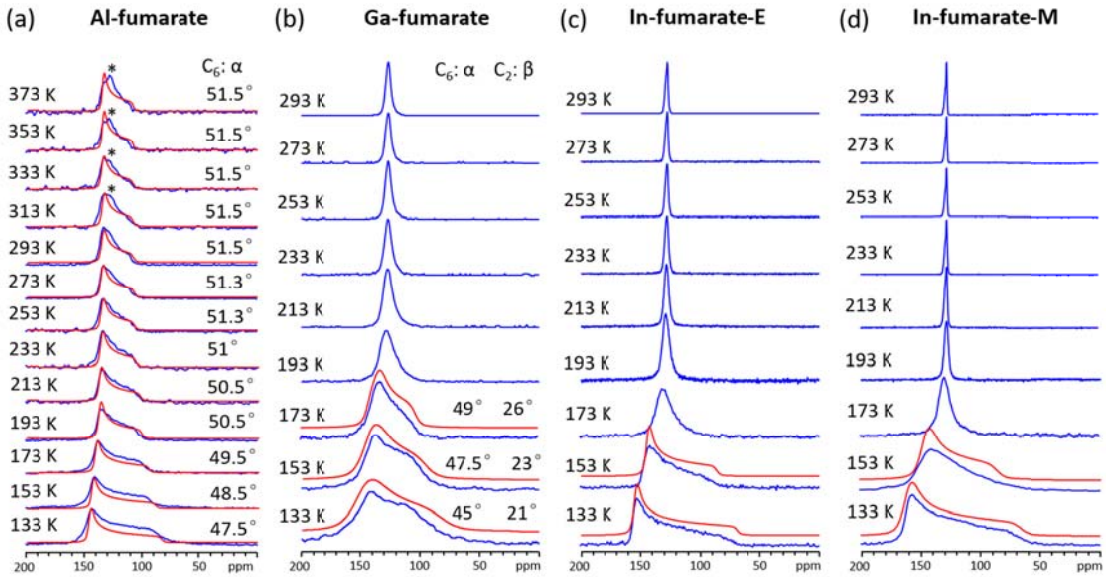

Figure 11. The experimental (blue) and motionally simulated (red) static VT ^{13}C NMR spectra of CO_2 adsorbed within Al-fumarate, Ga-fumarate, In-fumarate-E and In-fumarate-M are shown in (a), (b), (c), and (d), respectively. The motionally simulated powder patterns were generated using the EXPRESS software[43] and employed a fast rate of CO_2 motion (10^9 Hz). The CO_2 guest dynamics were modeled using two simultaneous motions: (i) a sixfold rotation (C_6) that corresponds to a localized rotational "wobbling" motion of CO_2 upon the adsorption site through the wobbling angle α, along with (ii) a twofold jumping (C_2) motion that describes a non-localized hopping or jumping of CO_2 through a hopping angle of β between two proximate adsorption sites. The asterisk (*) in (a) at high temperatures marks a sharp resonance at ca. 125 ppm that corresponds to gaseous, unbound CO_2. The uncertainty in α and β is estimated to be $\pm$ 0.2°.

As the temperature decreases from 293 to 193 K, the only discernable difference in the ^{13}C NMR spectra of CO_2 in Ga-fumarate is a continual broadening of the featureless resonance from a FWHH of 443 Hz to 1384 Hz. At 173 K, the observed ^{13}C resonance of CO_2 adsorbed in Ga-fumarate resembles a typical powder pattern, indicating that CO_2 guests now are participating in well-defined motions; the spectrum was simulated to

extract a Ω value of 40(1) ppm and a κ of 0.50(2) (Table S7). The powder pattern continues to broaden and change in appearance as the temperature decreases to 133K, where simulations show Ω is 68(1) ppm and κ is 0.88(2) (Table S7). Continued increases in Ω and κ as temperature decreases is a clear sign that adsorbed CO_2 molecules within Ga-fumarate are less dynamic at lower temperatures.

The observed ^{13}C NMR spectra of $^{13}CO_2$ adsorbed within In-fumarate-E and In-fumarate-M feature sharp isotropic resonances located at ca. 125 ppm (Figure 11(c) and (d)) at 293 K, with relatively narrow FWHHs of 283 Hz and 171 Hz, respectively, that indicate CO_2 undergoes fast isotropic tumbling inside In-fumarate-E and In-fumarate-M. A smaller measured FWHH value is reflective of more mobile CO_2 species and thus FWHH can be used as a qualitative measure to order the CO_2 binding strength within fumarate MOFs such that Al-fumarate > Ga-fumarate > In-fumarate-E > In-fumarate-M. This order is in good agreement with the CO_2 adsorption isotherms depicted in Figure 9(b). The broad ^{13}C NMR powder patterns indicating that CO_2 is participating in well-defined motions within In-fumarate-E and In-fumarate-M first appear at 153 K. The ^{13}C Ω value increases from 58(1) ppm at 153 K to 85(2) ppm at 133 K in In-fumarate-E, while the ^{13}C Ω value increases from 60(1) ppm at 153 K to 95(2) ppm at 133 K in In-fumarate-M (Table S7).

CO_2 dynamic studies. With knowledge of the ^{13}C NMR parameters for static CO_2,[74] the powder patterns of adsorbed $^{13}CO_2$ in Al- and Ga-fumarate MOFs were simulated[75]

to obtain accurate information regarding CO_2 motion (Figure 11). Simulations indicate that CO_2 molecules within Al-fumarate participate in a localized rotation or "wobbling" through an angle α upon the bridging hydroxyl adsorption site. This wobbling motion was modeled by a six-fold (C_6) rotation at a rate of 10^9 Hz (*i.e.*, in the NMR fast motion regime); this motional model is depicted in Figure 12(a) and (b). The wobbling angle α decreases from 51.5 ° to 47.5 ° as the temperature is reduced from 373 K to 133 K (Figure 11(a)), which indicates that the adsorbed CO_2 guests are less dynamic and sample a relatively smaller volume of space at lower temperatures when less thermal energy is available to compete with the adsorptive interaction. It is interesting to see no jumping or "hopping" of CO_2 between symmetry-equivalent adsorption sites in Al-fumarate, while hopping was observed in the structural analogue MIL-53-Al.[35] This is likely due to the larger pore structure of the Al-fumarate MOF (dimensions of *ca*. 12 x 12 Å), where the relatively longer distance between bridging hydroxyl adsorption sites prevents CO_2 hopping across the channel between these adsorption sites.

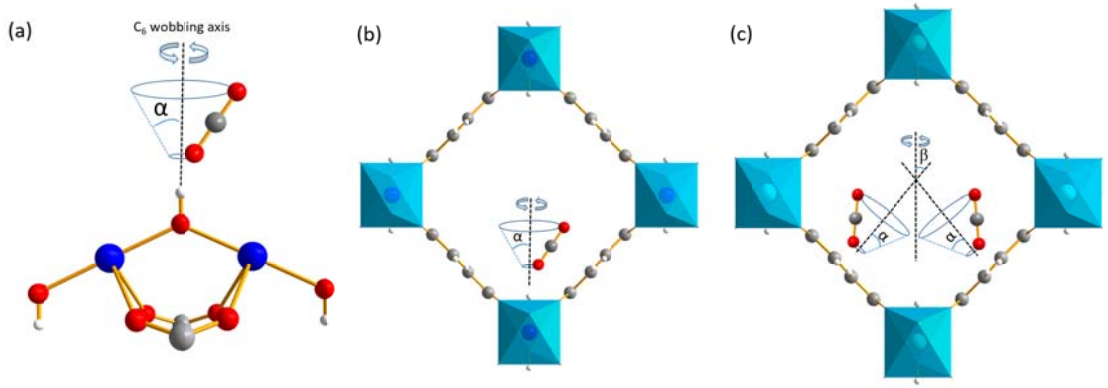

Figure 12. In (a), the localized C_6 rotational wobbling of CO_2 through an angle α about the CO_2 adsorption site (*i.e.,* the bridging hydroxyl group between SBUs) within Al-fumarate is shown. A schematic of how a single CO_2 guest wobbles upon adsorption sites in the channels of Al-fumarate is shown in (b). The localized wobbling (C_6 rotation through the angle α) and non-localized two site hopping (C_2 jumping through the angle β) of CO_2 within Ga-fumarate is illustrated in (c). The colors red, grey, white, dark blue and light blue correspond to oxygen, carbon, hydrogen, aluminum, and gallium, respectively.

The ^{13}C NMR spectrum of CO_2 adsorbed within Ga-fumarate only features a well-defined powder pattern at and below 173 K (Figure 11(b)), but motional information could still be obtained from these three low temperature spectra. Simulations reveal that, in addition to a localized wobbling through some angle α modeled by a C_6 rotation, adsorbed CO_2 guests also undergo a non-localized two-fold (C_2) hopping motion through an angle β between two adsorption sites. As the temperature decreases from 173 K to 133 K, the CO_2 wobbling angle α falls from 49 ° to 45 °, while the twofold hopping angle β is reduced from 26 ° to 21 °. These motional angle trends strongly hint that CO_2 molecules are significantly less dynamic at lower temperatures, although both types of dynamics remain in the fast motion regime (rate $\geq 10^7$ Hz). Recalling that ^1H-^{13}C CP NMR experiments suggested CO_2 adsorption sites in

Ga-fumarate are the hydrogen atoms of the organic fumarate linkers (*see above*), it follows that the twofold hopping of CO_2 must occur between different H atoms of the linkers. We suggest that CO_2 molecules within Ga-fumarate hop between two spatially proximate H atoms; many of these formate H atoms are only separated by distances ranging from ca. 5 Å to ca. 7 Å. Our proposed motional model for CO_2 within Ga-fumarate is pictured in Figure 12(c).

CO_2 adsorbed within both In-fumarate-E and –M yields an isotropic resonance at temperatures from 293 K down to ca. 173 K. Broad, well-defined ^{13}C powder patterns similar to those of CO_2 within Al-fumarate can be observed at temperatures of 153 and 133 K, with relatively larger span values in the In-fumarate MOFs. However, the ^{13}C powder patterns could only can be observed at two temperatures within a fairly tight range, and thus motional simulations were not possible and accurate CO_2 motional information could not be obtained for the In-fumarate MOFs at this time.

^{69}Ga, ^{71}Ga, and ^{115}In NMR of CO_2-loaded Ga-fumarate and In-fumarate. In all instances, these wideline metal NMR spectra indicate that the local environment about the metal center is not significantly influenced by CO_2 adsorption. See the Supporting Information for a full discussion.

Conclusions

The gallium and indium analogues of Al-fumarate, Ga-fumarate and In-fumarate, have been successfully synthesized using an experimentally-optimized solvothermal method. A variety of characterization techniques including synchrotron pXRD experiments, subsequent Rietveld refinements, IR spectroscopy, ^{1}H MAS NMR, and ultra-wideline Ga NMR were used to elucidate the true crystal structure of Ga-fumarate-H_2O. Ga- and In-fumarate are porous structural analogs of the Al-fumarate MOF. The relatively high BET surface areas and large, rigid pores of Ga- and In-fumarate point towards potential applications in fields such as gas storage, gas separation, and drug delivery. Hydrophilic and hydrophobic versions of In-fumarate can be produced depending on the solvent used in synthesis; hydrophobicity was successfully introduced within the In-fumarate-M framework by simply using methanol as the reaction solvent, leading to an *in situ* structural modification by replacing the –OH groups that bridge InO_6 units with $–OCH_3$ moieties pointing towards the pore interior.

CO_2 adsorption isotherms have been measured for these materials and reveal that both the Ga- and In-fumarate MOFs are well-suited for potential applications in CO_2 adsorption. The affinity for CO_2 follows the trend: Al-fumarate > Ga-fumarate > In-fumarate-E > In-fumarate-M. Static ^{1}H-^{13}C CP NMR spectra have confirmed that the CO_2 adsorption site in Al-fumarate is indeed the bridging hydroxyl group connecting the AlO_6 SBUs, while the adsorption sites in Ga-fumarate appear to be the hydrogen atoms

of the fumarate linkers lining the MOF channels. ^{13}C NMR experiments yield information on CO_2 adsorption and the complex CO_2 dynamics present in Al- and Ga-fumarate MOFs; in both MOFs, CO_2 locally rotates about the adsorption site, while in Ga-fumarate, CO_2 additionally hops between adjacent symmetry-equivalent adsorption sites. In both Al- and Ga-fumarate MOFs, the wobbling angle decreases with temperature, and in Ga-fumarate, the hopping angle also falls as temperature drops.

The described fumarate MOFs are fascinating materials with very promising applications, and increasingly detailed studies in the future regarding gas adsorption, gas separation, and catalysis will surely reveal more intriguing features and properties in these unique MOFs.

Acknowledgments

Access to the 21.1 T NMR spectrometer was provided by the National Ultrahigh-Field NMR Facility for Solids (http://nmr900.ca). Research described in this paper was performed using beamline 08B1-1 at the Canadian Light Source (CLS), which is supported by the Canadian Foundation for Innovation, the Natural Sciences and Engineering Research Council of Canada (NSERC), the National Research Council Canada, the Canadian Institutes of Health Research, the Government of Saskatchewan, Western Economic Diversification Canada, and the University of Saskatchewan. Periodic DFT

calculations were performed on a Graham supercomputer provided by Compute Ontario (www.computeontario.ca) and Compute Canada (www.computecanada.ca). Y.H. thanks NSERC for a Discovery Grant and a Discovery Accelerator Supplements Award. T.F. Acknowledges the support of the NSERC E. W. R. Steacie Memorial Fellowship (NSERC SMFSU 507347-17) and McGill University Dawson Scholarship. M.C. thanks the NSF of China (No. 21461004).

Supporting information. Powder X-ray diffraction data, TGA curves, $^{69/71}$Ga and ^{115}In solid-state NMR spectra and parameters, calculated $^{69/71}$Ga and ^{115}In NMR parameters, ^{1}H MAS and ^{1}H-^{13}C CP/MAS solid-state NMR spectra, static ^{1}H-^{13}C CP NMR spectra, tabulated ^{13}C NMR parameters of CO_2 within fumarate MOFs, IR spectra, SEM images, and BET surface areas.

References

(1) Zhou, H. C.; Kitagawa, S. Metal-Organic Frameworks (MOFs). *Chem. Soc. Rev.* **2014**, *43*, 5415-5418.

(2) Zhou, H.-C.; Long, J. R.; Yaghi, O. M. Introduction to Metal–Organic Frameworks. *Chem. Rev.* **2012**, *112*, 673-674.

(3) Notman, N. MOFs Find a Use.

http://www.chemistryworld.com/feature/mofs-find-a-use/2500508.article (accessed June 29, 2018).

(4) Mason, J. A.; Veenstra, M.; Long, J. R. Evaluating Metal-Organic Frameworks for Natural Gas Storage. *Chem. Sci.* **2014**, *5*, 32-51.

(5) Li, B.; Wen, H.-M.; Zhou, W.; Chen, B. Porous Metal–Organic Frameworks for Gas Storage and Separation: What, How, and Why? *J. Phys. Chem. Lett.* **2014**, *5*, 3468-3479.

(6) Sumida, K.; Rogow, D. L.; Mason, J. A.; McDonald, T. M.; Bloch, E. D.; Herm, Z. R.; Bae, T.-H.; Long, J. R. Carbon Dioxide Capture in Metal–Organic Frameworks. *Chem. Rev.* **2012**, *112*, 724-781.

(7) Qiu, S.; Xue, M.; Zhu, G. Metal-Organic Framework Membranes: From Synthesis to Separation Application. *Chem. Soc. Rev.* **2014**, *43*, 6116-6140.

(8) Li, J.-R.; Kuppler, R. J.; Zhou, H.-C. Selective Gas Adsorption and Separation in Metal-Organic Frameworks. *Chem. Soc. Rev.* **2009**, *38*, 1477-1504.

(9) Chughtai, A. H.; Ahmad, N.; Younus, H. A.; Laypkov, A.; Verpoort, F. Metal-Organic Frameworks: Versatile Heterogeneous Catalysts for Efficient Catalytic Organic Transformations. *Chem. Soc. Rev.* **2015**, *44*, 6804-6849.

(10) Liu, J.; Chen, L.; Cui, H.; Zhang, J.; Zhang, L.; Su, C.-Y. Applications of Metal-Organic Frameworks in Heterogeneous Supramolecular Catalysis. *Chem. Soc. Rev.* **2014**, *43*, 6011-6061.

(11) Horcajada, P.; Chalati, T.; Serre, C.; Gillet, B.; Sebrie, C.; Baati, T.; Eubank, J. F.; Heurtaux, D.; Clayette, P.; Kreuz, C.; Chang, J.-S.; Hwang, Y. K.; Marsaud, V.; Bories, P.-N.;

Cynober, L.; Gil, S.; Ferey, G.; Couvreur, P.; Gref, R. Porous Metal-Organic-Framework Nanoscale Carriers as a Potential Platform for Drug Delivery and Imaging. *Nat. Mater.* **2010**, *9*, 172-178.

(12) Vallet-Regí, M.; Balas, F.; Arcos, D. Mesoporous Materials for Drug Delivery. *Angew. Chem. Int. Ed.* **2007**, *46*, 7548-7558.

(13) Furukawa, H.; Cordova, K. E.; O'Keeffe, M.; Yaghi, O. M. The Chemistry and Applications of Metal-Organic Frameworks. *Science* **2013**, *341*, 1230444(1) - 1230444(12).

(14) James, S. L. Metal-Organic Frameworks. *Chem. Soc. Rev.* **2003**, *32*, 276-288.

(15) C. Kiener; U. Muller; Schubert, M. *Germany Pat.* **2007**, *WO2007/118841 A2*.

(16) Gaab, M.; Trukhan, N.; Maurer, S.; Gummaraju, R.; Müller, U. The Progression of Al-Based Metal-Organic Frameworks – from Academic Research to Industrial Production and Applications. *Microporous Mesoporous Mater.* **2012**, *157*, 131-136.

(17) Alvarez, E.; Guillou, N.; Martineau, C.; Bueken, B.; Van de Voorde, B.; Le Guillouzer, C.; Fabry, P.; Nouar, F.; Taulelle, F.; de Vos, D.; Chang, J.-S.; Cho, K. H.; Ramsahye, N.; Devic, T.; Daturi, M.; Maurin, G.; Serre, C. The Structure of the Aluminum Fumarate Metal–Organic Framework A520. *Angew. Chem. Int. Ed.* **2015**, *54*, 3664-3668.

(18) Loiseau, T.; Serre, C.; Huguenard, C.; Fink, G.; Taulelle, F.; Henry, M.; Bataille, T.; Férey, G. A Rationale for the Large Breathing of the Porous Aluminum Terephthalate (MIL-53) Upon Hydration. *Chem. Eur. J.* **2004**, *10*, 1373-1382.

(19) Serre, C.; Millange, F.; Thouvenot, C.; Noguès, M.; Marsolier, G.; Louër, D.; Férey, G.

Very Large Breathing Effect in the First Nanoporous Chromium(III)-Based Solids: MIL-53 or $Cr^{III}(OH)\cdot\{O_2C-C_6H_4-CO_2\}\cdot\{HO_2C-C_6H_4-CO_2H\}_X\cdot H_2O_Y$. *J. Am. Chem. Soc.* **2002**, *124*, 13519-13526.

(20) Bozbiyik, B.; Lannoeye, J.; De Vos, D. E.; Baron, G. V.; Denayer, J. F. M. Shape Selective Properties of the Al-Fumarate Metal-Organic Framework in the Adsorption and Separation of N-Alkanes, Iso-Alkanes, Cyclo-Alkanes and Aromatic Hydrocarbons. *Phys. Chem. Chem. Phys.* **2016**, *18*, 3294-3301.

(21) Coelho, J. A.; Ribeiro, A. M.; Ferreira, A. F. P.; Lucena, S. M. P.; Rodrigues, A. E.; Azevedo, D. C. S. D. Stability of an Al-Fumarate MOF and Its Potential for CO_2 Capture from Wet Stream. *Ind. Eng. Chem. Res.* **2016**, *55*, 2134-2143.

(22) Zhou, L.; Zhang, X.; Chen, Y. Facile Synthesis of Al-Fumarate Metal–Organic Framework Nano-Flakes and Their Highly Selective Adsorption of Volatile Organic Compounds. *Mater. Lett.* **2017**, *197*, 224-227.

(23) Chopra, S.; Dhumal, S.; Abeli, P.; Beaudry, R.; Almenar, E. Metal-Organic Frameworks Have Utility in Adsorption and Release of Ethylene and 1-Methylcyclopropene in Fresh Produce Packaging. *Postharvest Biol. Technol.* **2017**, *130*, 48-55.

(24) C. Kiener; U. Muller; Schubert, M. *US Pat.* **2009**, *US 12/297,666*.

(25) Karmakar, S.; Dechnik, J.; Janiak, C.; De, S. Aluminium Fumarate Metal-Organic Framework: A Super Adsorbent for Fluoride from Water. *J. Hazard. Mater.* **2016**, *303*, 10-20.

(26) Jeremias, F.; Frohlich, D.; Janiak, C.; Henninger, S. K. Advancement of Sorption-Based

Heat Transformation by a Metal Coating of Highly-Stable, Hydrophilic Aluminium Fumarate MOF. *RSC Adv.* **2014**, *4*, 24073-24082.

(27) Yot, P. G.; Vanduyfhuys, L.; Alvarez, E.; Rodriguez, J.; Itie, J.-P.; Fabry, P.; Guillou, N.; Devic, T.; Beurroies, I.; Llewellyn, P. L.; Van Speybroeck, V.; Serre, C.; Maurin, G. Mechanical Energy Storage Performance of an Aluminum Fumarate Metal-Organic Framework. *Chem. Sci.* **2016**, *7*, 446-450.

(28) Ruano, D.; Díaz-García, M.; Alfayate, A.; Sánchez-Sánchez, M. Nanocrystalline M–MOF-74 as Heterogeneous Catalysts in the Oxidation of Cyclohexene: Correlation of the Activity and Redox Potential. *ChemCatChem* **2015**, *7*, 674-681.

(29) Ravon, U.; Chaplais, G.; Chizallet, C.; Seyyedi, B.; Bonino, F.; Bordiga, S.; Bats, N.; Farrusseng, D. Investigation of Acid Centers in MIL-53(Al, Ga) for Bronsted-Type Catalysis: In Situ FTIR and Ab Initio Molecular Modeling. *ChemCatChem* **2010**, *2*, 1235-1238.

(30) Ramaswamy, P.; Wieme, J.; Alvarez, E.; Vanduyfhuys, L.; Itie, J.-P.; Fabry, P.; Van Speybroeck, V.; Serre, C.; Yot, P. G.; Maurin, G. Mechanical Properties of a Gallium Fumarate Metal-Organic Framework: A Joint Experimental-Modelling Exploration. *J. Mater. Chem. A* **2017**, *5*, 11047-11054.

(31) Chaplais, G.; Simon-Masseron, A.; Porcher, F.; Lecomte, C.; Bazer-Bachi, D.; Bats, N.; Patarin, J. IM-19: A New Flexible Microporous Gallium Based-MOF Framework with Pressure- and Temperature-Dependent Openings. *Phys. Chem. Chem. Phys.* **2009**, *11*, 5241-5245.

(32) Volkringer, C.; Loiseau, T.; Guillou, N.; Ferey, G.; Elkaim, E.; Vimont, A. XRD and IR

Structural Investigations of a Particular Breathing Effect in the MOF-Type Gallium Terephthalate MIL-53(Ga). *Dalton Trans.* **2009**, *12*, 2241-2249.

(33) Ibrahim, B.; Lucier, B. E. G.; Xu, J.; He, P.; Huang, Y. Investigating Adsorption of Organic Compounds in Metal-Organic Framework MIL-53. *Can. J. Chem.* **2015**, *93*, 960-969.

(34) Zhang, Y.; Lucier, B. E. G.; Terskikh, V. V.; Zheng, R.; Huang, Y. Tracking the Evolution and Differences between Guest-Induced Phases of Ga-MIL-53 Via Ultra-Wideline $^{69/71}$Ga Solid-State NMR Spectroscopy. *Solid State Nucl. Magn. Reson.* **2017**, *84*, 118-131.

(35) Zhang, Y.; Lucier, B. E. G.; Huang, Y. Deducing CO_2 Motion, Adsorption Locations and Binding Strengths in a Flexible Metal-Organic Framework without Open Metal Sites. *Phys. Chem. Chem. Phys.* **2016**, *18*, 8327-8341.

(36) Stavitski, E.; Pidko, E. A.; Couck, S.; Remy, T.; Hensen, E. J. M.; Weckhuysen, B. M.; Denayer, J.; Gascon, J.; Kapteijn, F. Complexity Behind CO_2 Capture on NH_2-MIL-53(Al). *Langmuir* **2011**, *27*, 3970-3976.

(37) Ramsahye, N. A.; Maurin, G.; Bourrelly, S.; Llewellyn, P. L.; Serre, C.; Loiseau, T.; Devic, T.; Férey, G. Probing the Adsorption Sites for CO_2 in Metal Organic Frameworks Materials MIL-53 (Al, Cr) and MIL-47 (V) by Density Functional Theory. *J. Phys. Chem. C* **2008**, *112*, 514-520.

(38) Lucier, B. E. G.; Chen, S.; Huang, Y. Characterization of Metal–Organic Frameworks: Unlocking the Potential of Solid-State NMR. *Acc. Chem. Res.* **2018**, *51*, 319-330.

(39) Pyykkö, P. Year-2008 Nuclear Quadrupole Moments. *Mol. Phys.* **2008**, *106*,

1965-1974.

(40) Volkringer, C.; Loiseau, T.; Férey, G.; Morais, C. M.; Taulelle, F.; Montouillout, V.; Massiot, D. Synthesis, Crystal Structure and ^{71}Ga Solid State NMR of a MOF-Type Gallium Trimesate (MIL-96) with M_3-Oxo Bridged Trinuclear Units and a Hexagonal 18-Ring Network. *Microporous Mesoporous Mater.* **2007**, *105*, 111-117.

(41) Hajjar, R.; Volkringer, C.; Loiseau, T.; Guillou, N.; Marrot, J.; Férey, G.; Margiolaki, I.; Fink, G.; Morais, C.; Taulelle, F. 71ga Slow-Ctmas Nmr and Crystal Structures of MOF-Type Gallium Carboxylates with Infinite Edge-Sharing Octahedra Chains (MIL-120 and MIL-124). *Chem. Mater.* **2011**, *23*, 39-47.

(42) Johnston, K. E.; O'Keefe, C. A.; Gauvin, R. M.; Trebosc, J.; Delevoye, L.; Amoureux, J. P.; Popoff, N.; Taoufik, M.; Oudatchin, K.; Schurko, R. W. A Study of Transition-Metal Organometallic Complexes Combining ^{35}Cl Solid-State NMR Spectroscopy and ^{35}Cl NQR Spectroscopy and First-Principles DFT Calculations. *Chem. Eur. J.* **2013**, *19*, 12396-12414.

(43) Lucier, B. E. G.; Reidel, A. R.; Schurko, R. W. Multinuclear Solid-State NMR of Square-Planar Platinum Complexes - Cisplatin and Related Systems. *Can. J. Chem.* **2011**, *89*, 919-937.

(44) Hamaed, H.; Johnston, K. E.; Cooper, B. F. T.; Terskikh, V. V.; Ye, E.; Macdonald, C. L. B.; Arnold, D. C.; Schurko, R. W. A ^{115}In Solid-State NMR Study of Low Oxidation-State Indium Complexes. *Chem. Sci.* **2014**, *5*, 982-995.

(45) Lo, A. Y. H.; Jurca, T.; Richeson, D. S.; Bryce, D. L. Multinuclear Solid-State Magnetic Resonance Study of In^+ and Ag^+ in Neutral Weakly Coordinating Environments. *J. Phys.*

Chem. Lett. **2010**, *1*, 3078-3084.

(46) Chen, F.; Ma, G.; Bernard, G. M.; Cavell, R. G.; McDonald, R.; Ferguson, M. J.; Wasylishen, R. E. Solid-State ^{115}In and ^{31}P NMR Studies of Triarylphosphine Indium Trihalide Adducts. *J. Am. Chem. Soc.* **2010**, *132*, 5479-5493.

(47) Chen, F.; Ma, G.; Cavell, R. G.; Terskikh, V. V.; Wasylishen, R. E. Solid-State ^{115}In Nmr Study of Indium Coordination Complexes. *Chem. Commun.* **2008**, 5933-5935.

(48) He, P.; Lucier, B. E. G.; Terskikh, V. V.; Shi, Q.; Dong, J.; Chu, Y.; Zheng, A.; Sutrisno, A.; Huang, Y. Spies within Metal-Organic Frameworks: Investigating Metal Centers Using Solid-State NMR. *J. Phys. Chem. C* **2014**, *118*, 23728-23744.

(49) Huang, Y.; Xu, J.; Gul-E-Noor, F.; He, P., Metal-Organic Frameworks: NMR Studies of Quadrupolar Nuclei. In *Encyclopedia of Inorganic and Bioinorganic Chemistry*, John Wiley & Sons, Ltd: 2011. DOI: 10.1002/9781119951438.eibc2225

(50) Fernandez, C. A.; Nune, S. K.; Annapureddy, H. V.; Dang, L. X.; McGrail, B. P.; Zheng, F.; Polikarpov, E.; King, D. L.; Freeman, C.; Brooks, K. P. Hydrophobic and Moisture-Stable Metal-Organic Frameworks. *Dalton Trans.* **2015**, *44*, 13490-13497.

(51) Keskin, S.; van Heest, T. M.; Sholl, D. S. Can Metal–Organic Framework Materials Play a Useful Role in Large-Scale Carbon Dioxide Separations? *ChemSusChem* **2010**, *3*, 879-891.

(52) Burtch, N. C.; Jasuja, H.; Walton, K. S. Water Stability and Adsorption in Metal–Organic Frameworks. *Chem. Rev.* **2014**, *114*, 10575-10612.

(53) Howarth, A. J.; Liu, Y.; Li, P.; Li, Z.; Wang, T. C.; Hupp, J. T.; Farha, O. K. Chemical,

Thermal and Mechanical Stabilities of Metal–Organic Frameworks. *Nat. Rev. Mater.* **2016**, *1*, 15018(1) - 15018(15).

(54) Coates, J., Interpretation of Infrared Spectra, a Practical Approach. In *Encyclopedia of Analytical Chemistry*, John Wiley & Sons, Ltd: 2006. DOI: 10.1002/9780470027318.a5606

(55) Boutin, A.; Bousquet, D.; Ortiz, A. U.; Coudert, F.-X.; Fuchs, A. H.; Ballandras, A.; Weber, G.; Bezverkhyy, I.; Bellat, J.-P.; Ortiz, G.; Chaplais, G.; Paillaud, J.-L.; Marichal, C.; Nouali, H.; Patarin, J. Temperature-Induced Structural Transitions in the Gallium-Based MIL-53 Metal–Organic Framework. *J. Phys. Chem. C* **2013**, *117*, 8180-8188.

(56) Liu, L.; Wang, X.; Jacobson, A. J. AlF • 1,4-Benzenedicarboxylate: Synthesis and Absorption Properties. *Dalton Trans.* **2010**, *39*, 1722-1725.

(57) Barthelet, K.; Marrot, J.; Riou, D.; Férey, G. A Breathing Hybrid Organic–Inorganic Solid with Very Large Pores and High Magnetic Characteristics. *Angew. Chem. Int. Ed.* **2002**, *41*, 281-284.

(58) Kim, M.; Cahill, J. F.; Fei, H.; Prather, K. A.; Cohen, S. M. Postsynthetic Ligand and Cation Exchange in Robust Metal–Organic Frameworks. *J. Am. Chem. Soc.* **2012**, *134*, 18082-18088.

(59) Hoffmann, H.; Debowski, M.; Müller, P.; Paasch, S.; Senkovska, I.; Kaskel, S.; Brunner, E. Solid-State NMR Spectroscopy of Metal–Organic Framework Compounds (MOFs). *Materials* **2012**, *5*, 2537-2572.

(60) Kong, X.; Scott, E.; Ding, W.; Mason, J. A.; Long, J. R.; Reimer, J. A. CO_2 Dynamics in a

Metal–Organic Framework with Open Metal Sites. *J. Am. Chem. Soc.* **2012**, *134*, 14341-14344.

(61) Gul-E-Noor, F.; Mendt, M.; Michel, D.; Pöppl, A.; Krautscheid, H.; Haase, J.; Bertmer, M. Adsorption of Small Molecules on $Cu_3(btc)_2$ and $Cu_{3-x}Zn_x(btc)_2$ Metal–Organic Frameworks (MOF) as Studied by Solid-State NMR. *J. Phys. Chem. C* **2013**, *117*, 7703-7712.

(62) Lin, L.-C.; Kim, J.; Kong, X.; Scott, E.; McDonald, T. M.; Long, J. R.; Reimer, J. A.; Smit, B. Understanding CO_2 Dynamics in Metal–Organic Frameworks with Open Metal Sites. *Angew. Chem. Int. Ed.* **2013**, *52*, 4410-4413.

(63) Peksa, M.; Burrekaew, S.; Schmid, R.; Lang, J.; Stallmach, F. Rotational and Translational Dynamics of CO_2 Adsorbed in MOF $Zn_2(bdc)_2(dabco)$. *Microporous Mesoporous Mater.* **2015**, *216*, 75-81.

(64) Masala, A.; Grifasi, F.; Atzori, C.; Vitillo, J. G.; Mino, L.; Bonino, F.; Chierotti, M. R.; Bordiga, S. CO_2 Adsorption Sites in UTSA-16: Multitechnique Approach. *J. Phys. Chem. C* **2016**, *120*, 12068-12074.

(65) Lu, Y.; Lucier, B. E. G.; Zhang, Y.; Ren, P.; Zheng, A.; Huang, Y. Sizable Dynamics in Small Pores: CO_2 Location and Motion in the α-Mg Formate Metal-Organic Framework. *Phys. Chem. Chem. Phys.* **2017**, *19*, 6130-6141.

(66) Forse, A. C.; Gonzalez, M. I.; Siegelman, R. L.; Witherspoon, V. J.; Jawahery, S.; Mercado, R.; Milner, P. J.; Martell, J. D.; Smit, B.; Blümich, B.; Long, J. R.; Reimer, J. A. Unexpected Diffusion Anisotropy of Carbon Dioxide in the Metal–Organic Framework

Zn_2(dobpdc). *J. Am. Chem. Soc.* **2018**, *140*, 1663-1673.

(67) Chen, M.; Chen, S.; Chen, W.; Lucier, B. E. G.; Zhang, Y.; Zheng, A.; Huang, Y. Analyzing Gas Adsorption in an Amide-Functionalized Metal Organic Framework: Are the Carbonyl or Amine Groups Responsible? *Chem. Mater.* **2018**, *30*, 3613-3617.

(68) Bon, V.; Pallmann, J.; Eisbein, E.; Hoffmann, H. C.; Senkovska, I.; Schwedler, I.; Schneemann, A.; Henke, S.; Wallacher, D.; Fischer, R. A.; Seifert, G.; Brunner, E.; Kaskel, S. Characteristics of Flexibility in Metal-Organic Framework Solid Solutions of Composition $Zn_2(bme\text{-}bdc)_X(db\text{-}bdc)_{2\text{-}X}dabco_N$: In Situ Powder X-Ray Diffraction, In Situ NMR Spectroscopy, and Molecular Dynamics Simulations. *Microporous Mesoporous Mater.* **2015**, *216*, 64-74.

(69) Marti, R. M.; Howe, J. D.; Morelock, C. R.; Conradi, M. S.; Walton, K. S.; Sholl, D. S.; Hayes, S. E. CO_2 Dynamics in Pure and Mixed-Metal MOFs with Open Metal Sites. *J. Phys. Chem. C* **2017**, *121*, 25778-25787.

(70) Baek, S. B.; Lee, H. C. ^{13}C NMR Study of CO_2 Adsorbed in Highly Flexible Porous Metal-Organic Frameworks. *Bull. Korean Chem. Soc.* **2016**, *37*, 588-591.

(71) Bassanetti, I.; Comotti, A.; Sozzani, P.; Bracco, S.; Calestani, G.; Mezzadri, F.; Marchio, L. Porous Molecular Crystals by Macrocyclic Coordination Supramolecules. *J. Am. Chem. Soc.* **2014**, *136*, 14883-14895.

(72) Lucier, B. E. G.; Zhang, Y.; Huang, Y. Complete Multinuclear Solid‐State NMR of Metal‐Organic Frameworks: The Case of α-Mg-Formate. *Concepts Magn. Reson. Part A* **2017**, DOI: 10.1002/cmr.a.21410.

(73) Chen, S.; Lucier, B. E. G.; Boyle, P. D.; Huang, Y. Understanding the Fascinating Origins of CO_2 Adsorption and Dynamics in MOFs. *Chem. Mater.* **2016**, *28*, 5829-5846.

(74) Beeler, A. J.; Orendt, A. M.; Grant, D. M.; Cutts, P. W.; Michl, J.; Zilm, K. W.; Downing, J. W.; Facelli, J. C.; Schindler, M. S.; Kutzelnigg, W. Low-Temperature ^{13}C Magnetic Resonance in Solids. 3. Linear and Pseudolinear Molecules. *J. Am. Chem. Soc.* **1984**, *106*, 7672-7676.

(75) Vold, R. L.; Hoatson, G. L. Effects of Jump Dynamics on Solid State Nuclear Magnetic Resonance Line Shapes and Spin Relaxation Times. *J. Magn. Reson.* **2009**, *198*, 57-72.

Table of Contents Graphic